Implementation of spatial diversity and multiplexing on an open source 802.11 SDR platform

Cedric Den Haese

Student number: 01602866

Supervisor: Prof. dr. ir. Ingrid Moerman
Counsellors: Dr. Xianjun Jiao, Dr. Wei Liu, Dr. ir. Michael Mehari

Implementation of spatial diversity and multiplexing on an open source 802.11 SDR platform

Cedric Den Haese
Student number: 01602866

GHENT
UNIVERSITY

Acknowledgements

Implementation of spatial diversity and multiplexing on an open source 802.11 platform

by
Cedric Den Haese

Master's dissertation submitted in order to obtain the academic degree of
Master of Science in Electrical Engineering - Communication and Information Technology

Academic year 2020-2021

Supervisor: Prof. dr. ir. Ingrid Moerman
Counsellors: Dr. Xianjun Jiao, Dr. Wei Liu, Dr. ir. Michael Mehari

Faculty of Engineering and Architecture
Ghent University

Department of Information Technology
Chair: Prof. dr. ir. Bart Dhoedt

Summary

The ever increasing demand for bandwidth in wireless communication has pushed new standards to look for better and more complex signal processing techniques in order to increase the obtainable throughput. Most of these techniques are related to the use of multiple antennas for both transmission and reception. In this work, several approaches to improve the reliability and throughput of an open source IEEE 802.11 communication system using multiple antennas are implemented on an SDR platform, and their performance is evaluated in end-to-end communication scenarios. First, spatial diversity is used at the receiver side and evaluated in a controlled environment. Measurements show that combining the input of multiple antennas can aid in sustaining higher throughputs in different scenarios. Next, spatial diversity is also explored at the transmitter side, and measurements are conducted in the same controlled environment to assess its influence on communication performance. It is shown that transmit diversity helps in increasing the reliability of wireless link as sudden drops in throughput can be mitigated better. Finally, the SDR design is extended with the capability to use spatial multiplexing, or also known as MIMO, for transmission. The new MIMO transmission is evaluated in a real life scenario and the resulting increase in throughput is found to correspond to the theoretically expected value.

Keywords
SDR, FGPA, spatial diversity, spatial multiplexing, MIMO

Implementation of spatial diversity and multiplexing on an open source 802.11 SDR platform

Cedric Den Haese

Supervisors: Ingrid Moerman, Xianjun Jiao, Wei Liu, Michael Mehari

Abstract - This article discusses the implementation and evaluation of spatial diversity and spatial multiplexing on the openwifi platform.

Keywords - SDR, FPGA, spatial diversity, spatial multiplexing, MIMO

I. Introduction

THE ever increasing demand for bandwidth in wireless communication has pushed new standards to look for better and more complex signal processing techniques in order to increase the obtainable throughput. Most of these techniques are related to the use of multiple antennas for both transmission and reception. Two distinct techniques, called spatial diversity and spatial multiplexing, are possible.

The aim is to examine the influence of these techniques when applied to Wi-Fi. To this end, the openwifi platform is used. This is an open source SDR implementation of Wi-Fi which is compatible with devices using the 802.11a/g/n standards. Openwifi implements the physical layer and lower MAC layer, whereas the mac80211 subsystem from the Linux kernel is used to provide upper MAC layer functionality.

In this abstract, the implementation of both methods on the openwifi platform is discussed. In addition, measurements are provided to show the benefit of each of these techniques.

II. Spatial diversity

One of the major challenges in the design of any wireless communication system is the occurrence of fading, which corresponds to rapid variations in the signal level at the receiver. Spatial diversity is one of the techniques which can be used to mitigate the effect of this phenomenon. By using multiple antennas, the robustness and reliability of the wireless channel can be increased when fading occurs.

Spatial diversity is a technique which can be applied independently at the receiver or transmitter. Applied to implementation on the openwifi platform, this implies that the 802.11 standard does not necessarily need to be followed for the approach to still be interoperable with other 802.11 systems.

A. Receiver diversity

At the receiver, the use of spatial diversity relates to how the signals from each antenna are combined. Well-known approaches are maximal ratio combining, equal gain combining and selection combining. In maximal ratio combining, complex symbols from each antenna are averaged, taking into account the signal-to-noise ratio (SNR) on each symbol, in order to provide the final symbol. In equal gain combining, the same averaging operation is performed, but this time each symbol contributes equally to the average. In selection combining, no averaging is performed, but rather the single antenna with the best SNR at that time is used for reception.

An advantage of maximal ratio and equal gain combining over selection combining is that multiple antennas are used instead of only a single one. This implies that more signal power will be available at the receiver for the symbol decision. Although the maximal ratio combining operation is theoretically better than equal gain combining, this gain is only marginal. Additionally, maximal ratio combining requires calculating the SNR for each available antenna. Since the additional gain from maximal ration combining does not justify the added implementation complexity, the choice was made to implement equal gain combining on the openwifi platform. Note that the hardware boards used by openwifi are limited to two antennas.

To test the performance of the equal

gain combining implementation, measurements were done on a setup where the openwifi SDR board is connected to a commercial off-the-shelf (COTS) device via coax cables. The attenuation on the two receive ports on the openwifi board is configurable, such that the influence of fading can be emulated independently on each antenna. For different attenuation settings, the transmit rate which is most frequently used from the COTS device to the openwifi board is then measured. Since the COTS device operates on Linux, the used transmit rate will be selected by the *minstrel* rate selection algorithm inside the mac80211 subsystem. As each Wi-Fi packet has to be acknowledged by the receiver, information on whether a transmission was successful or not can be used by *minstrel* to decide which transmit rate will result in the largest throughput, which is a trade-off between the packet success rate and the bitrate corresponding to the used transmit rate. A better receiver will thus allow transmission with higher bitrate.
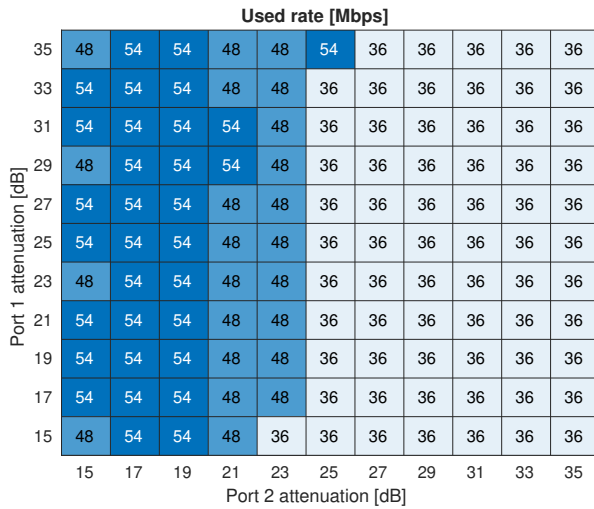

Figure 1: Selected transmit rate at COTS device when using a single antenna

The resulting measurements in case only a single antenna is used are shown in figure 1. On this figure, the selected transmit rate is given for the different settings on each of the attenuators. As only a single antenna is used at any given time, the attenuation on port 1 does not influence the selected rate.

By moving to the equal gain combining implementation, figure 2 is obtained. It can be

seen that now higher rates can be supported, if there is an asymmetrical attenuation on both ports. Translated to a real world example, this implies that if fading were to occur at only a single antenna, the signal received at the other antenna can still compensate for the loss in signal power to provide the receiver with enough information to decode the signal. If both antennas are subject to fading, the transmit rate will of course also start to drop. But statistically speaking, it is less likely for both antennas to experience fading at the same time than it is for a single antenna. On average, this implies that the wireless channel will be able to sustain a higher transmit rate than it would be possible with only a single antenna.
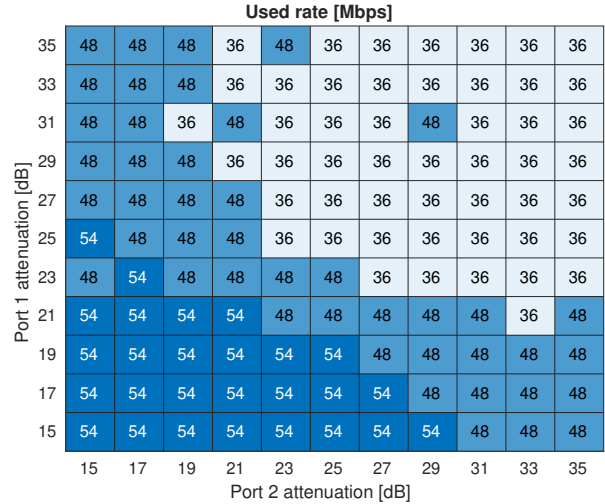
Figure 2: Selected transmit rate at COTS device when using two antennas

B. TRANSMITTER DIVERSITY

Diversity can also be applied at the transmitter side. Applied to Wi-Fi, the 802.11 standard specifies cyclic shift diversity (CSD), in which the signals transmitted on each antenna are obtained by cyclically shifting the values inside each OFDM symbol. The shift has to be applied cyclically instead of linearly in order to avoid issues with inter-block interference.

The implementation of CSD on the openwifi platform was evaluated on the same testbed as the receiver diversity implementation. However, this time the received signal strength indication (RSSI) and channel state information (CSI) were measured at the COTS device

instead of the used transmit rate. Figure 3 shows the obtained RSSI measurements. On this figure, the reference measurements where only a single antenna is used are included as well (ANT0 and ANT1). The other observations correspond to the application of CSD, where the number represents the number of samples that were cyclically shifted. It can be seen that simply using both antennas (observation CSD0) results in a gain of around 6 dB, whereas application of CSD results in only 3 dB of gain.

Figure 3: RSSI measurement for different CSD values

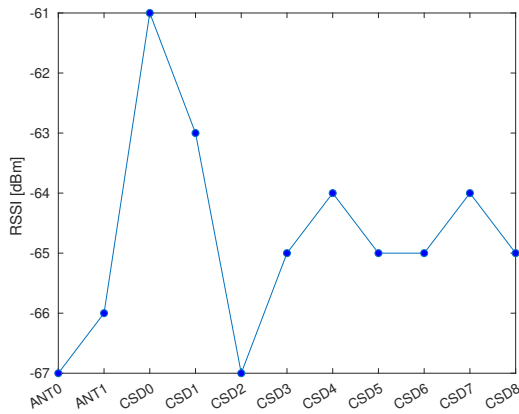In both cases, a 3 dB increase is to be expected due to a doubling of the transmit power. The additional 3 dB in case no CSD is applied comes from the fact that the signals from the two antennas are coherent, which implies that constructive interference will occur. However, it has to be taken into account that this measurement was obtained in a setup where the antenna ports were connected through cabling of the same length: in real world applications, the expected RSSI might differ largely, depending on the position of the receiver and the wireless environment. Due to the coherence relationship between both antennas, destructive coherence is just as likely to occur, in which case the RSSI can theoretically drop to minus infinity. For that reason, the introduction of CSD makes the wireless connection more robust: by destroying the coherence relation, no constructive or destructive interference will occur. The maximal RSSI gain will be smaller, but more stable.

Another effect of the application of cyclic shift diversity is the introduction of additional frequency selective fading. This effect is due to the fact that CSD corresponds to the introduction of a second, but delayed path arriving at the receiver. The corresponding measurements are shown on figure 4. Although the channel coefficients on some subcarriers are reduced, some subcarriers can actually see an increase. Due to sufficient interleaving and coding, this additional frequency selectivity does not introduce any problems.
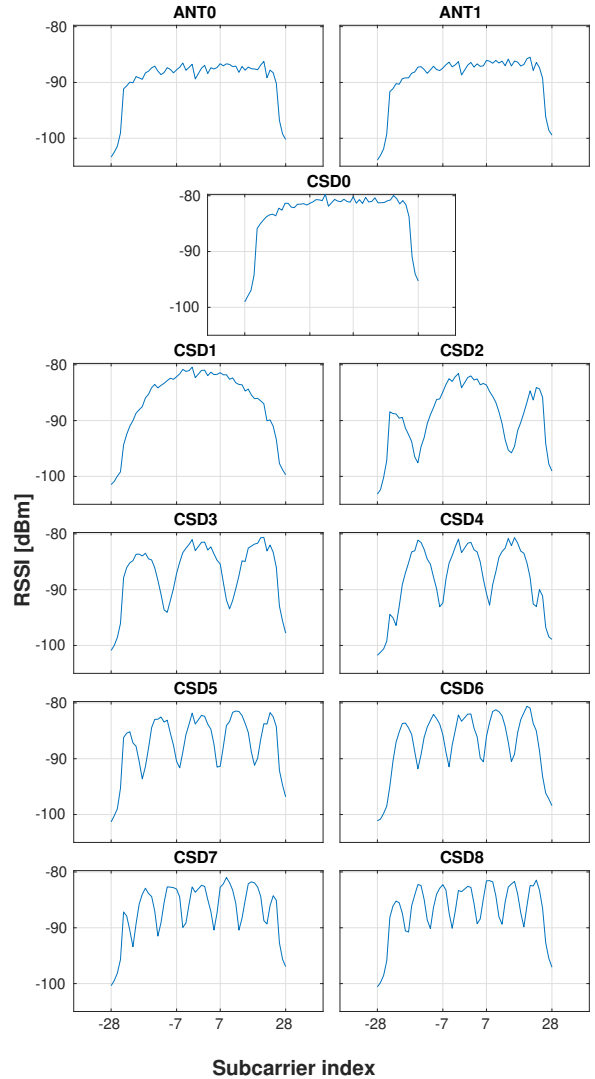

Figure 4: CSI measurement for different CSD values

III. Spatial Multiplexing

Another use of multiple antennas is called spatial multiplexing, which is better known as multiple-in multiple-out (MIMO). In this case, multipath transmission can be used to increase

the throughput over a wireless channel, compared to spatial diversity, where the goal was to increase the reliability of the channel. By using MIMO, the throughput can now be increased linearly with the minimal number of antennas at either the receiver or the transmitter.

Since MIMO requires modifications at both the receiver and transmitter, it is best to stick to the 802.11 standard in order to remain interoperable with other devices. For implementation on the openwifi platform, only MIMO transmission has been implemented in this thesis. More specifically, the transmission rates that use a 2x2 MIMO configuration with equal modulation from the 802.11n standard have been implemented.

The implementation of the MIMO transmission rates have been tested in a home environment, with another COTS device which is able to receive MIMO. The corresponding throughput was measured using the *iperf* tool over UDP. An increase in throughput was measured when enabling the new MIMO transmission rates on the openwifi board, going from 33,1 Mbits/sec to 44,8 Mbits/sec. Although this does not correspond to doubling the throughput, the measured values are still to be expected. Taking into account the additional overhead for medium access control (i.e. various inter frame spacing, and waiting period due to contention), an increase in the maximal physical bitrate will not lead to a linearly proportional increase in the overall throughput.

IV. CONCLUSION

Measurements on the openwifi platform have validated the advantages of using multiple antennas on an 802.11 system. Additionally, the benefits of openwifi as a research platform for experimenting with Wi-Fi have been demonstrated. Future research can profit from the open source nature of the openwifi platform to research modifications from the physical layer up to the MAC layer.

Contents

List of Figures

List of Abbreviations

FPGA Field Programmable Gate Array. 2, 3, 9, 19, 26, 38, 39

GI guard interval. ix, 9, 11, 17, 20, 24, 26, 41

IBI inter-block interference. 10, 11, 24

IDFT Inverse Discrete Fourier Transform. 9, 14, 24–27, 35, 36, 39

ISI intersymbol interference. 9

L-LTF legacy long training field. 13, 14

L-STF legacy short training field. 13

LO local oscillator. 12

LOS line-of-sight. 7

LUT lookup table. 36–38

MAC medium access control. 2, 3, 16

MCS modulation and coding scheme. x, 34–41

MIMO Multiple-Input Multiple-Output. ix, x, 4, 5, 31–36, 38–40, 42–44

MMSE minimun mean square error. 12

MU-MIMO multi-user MIMO. 5, 43

OFDM Orthogonal Frequency Division Multiplexing. ix, 3–6, 8–14, 16, 20, 21, 24–27, 38, 41, 47

OFDMA orthogonal frequency division multiple access. 43

PAPR peak-to-average power ratio. 3

PD phase diversity. 24

PLCP physical layer convergence protocol. xii

PPDU PLCP protocol data unit. 14, 20, 21, 34

PSDU Physical layer service data unit. 20

QAM quadrature amplitude modulation. 9, 34, 37, 38

ROM read only memory. 38

RSSI received signal strenght indicator. ix, 22, 28, 29

SDR Software Defined Radio. ix, 1–3, 21, 22, 29, 35, 39, 43

SFO sampling frequency offset. ix, 12, 13, 20

SIFS Short Interframe Spacing. 3, 28, 41

SISO Single-Input Single-Output. 33

SNR signal to noise ratio. 12, 17–19, 25, 29, 31, 33

SoC System on Chip. 3

STBC Space-Time Block Code. 16, 35

ZF zero forcing. 12

Chapter 1

Introduction

In recent years, Software Defined Radio (SDR) has been widely used for research in the field of wireless communication. In SDR, software is used to replace the components of a radio communication system that were usually implemented in hardware (such as filters, modulators/demodulators, etc.). The use of SDR provides many advantages. For manufacturers, SDR enables the development of a family of radio systems on a common platform, where code can be reused across different products. This reduces both the development costs and the time to market for new systems. Additionally, bug fixes can be applied to already deployed systems by reprogramming them, thus making maintenance simpler. The use of SDR platforms is also advantageous to researchers: the ability to reprogram the device allows to quickly modify the devices behaviour, such that the influence of different design choices on the communication performance can be verified faster. On the other hand, most of the limitations of SDR with regards to their reusability are fixed by the unavoidably analog part of the design. For example, the antenna(s) that are used need to be matched to a wide range of frequencies to support different applications. Otherwise, communication performance can be poor due to suboptimal power delivery to and reception from the antenna.
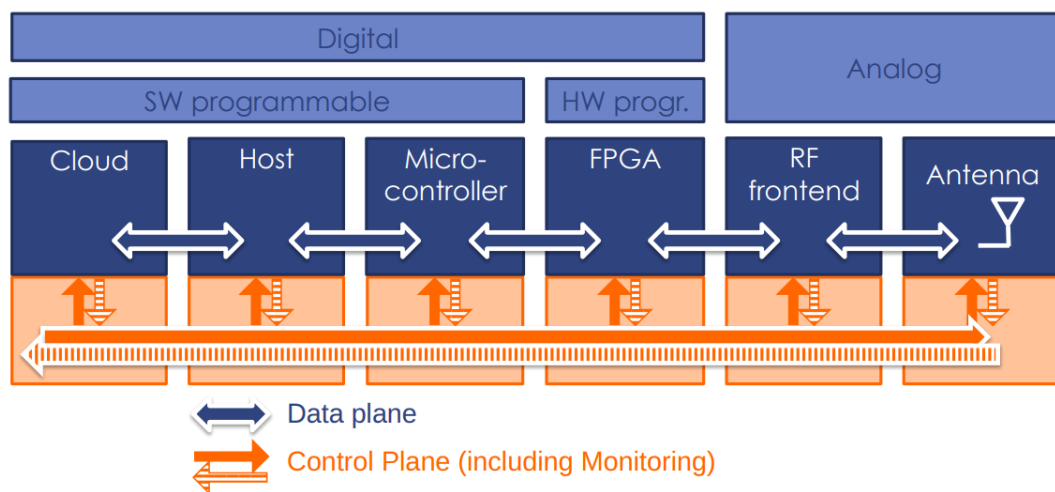
Figure 1.1: General overview of SDR architecture [1]

The architecture of an SDR system typically looks like figure 1.1. At the start of the communication chain is an RF frontend, which picks up analog radio signals with its antenna(s).

1

The RF frontend is very flexible, where parameters such as the carrier frequency, filtering and analog gain can be configured at runtime, as to accommodate different specifications from different standards. The analog signals from the RF frontend are sampled, which typically happens at a fixed sampling rate. These digital samples are then handed over to an FPGA, which is a hardware component that can be reconfigured to realize any digital function. In application to SDR, the FPGA can be responsible for several digital processing steps. An example includes the Fast Fourier Transform (FFT), as this can benefit from the parallelism inherent to FPGAs. The next block of the SDR architecture is the microcontroller, which is used for any additional sequential processing steps. Additionally, a host PC can be included in the architecture as well. Finally, some functionality can also be transferred to the cloud.
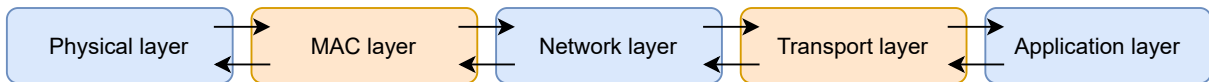
Figure 1.2: The OSI 5 layer model

The functional assignment of each of the blocks in the SDR architecture is best explained using the 5 layer OSI model (figure 1.2), where each layer is responsible for a subset of the tasks needed for end-to-end communication. Here, SDR technology is typically used for the implementation of the physical and MAC layer. The first option for the implementation of a wireless standard using SDR technology is to use an entirely host-controlled architecture, where all of the functionality from the high level physical layer and upwards is the responsibility of a host PC. In this case, the hardware is only responsible for up- and downconversion of the RF signals. The advantage of this approach is that code development becomes a lot easier, as no embedded or FPGA programming is required. However, this architecture needs to take into account the interface delay that is caused by the connection between hardware and host. This connection is typically a USB or Ethernet connection, and the delay in round-trip communication between hardware and host can be too large for certain applications. In this case, a design where more functionality is assigned to the hardware is necessary. Depending on the application, different functional assignments of the hardware to the OSI layers are possible, as can be seen on figure 1.3. The advantage of the increased hardware processing is that the interface delay can be moved to the higher layers of the OSI model, which are less sensitive to this delay. However, the development of such platforms becomes increasingly difficult when more and more functionality is assigned to the FPGA.
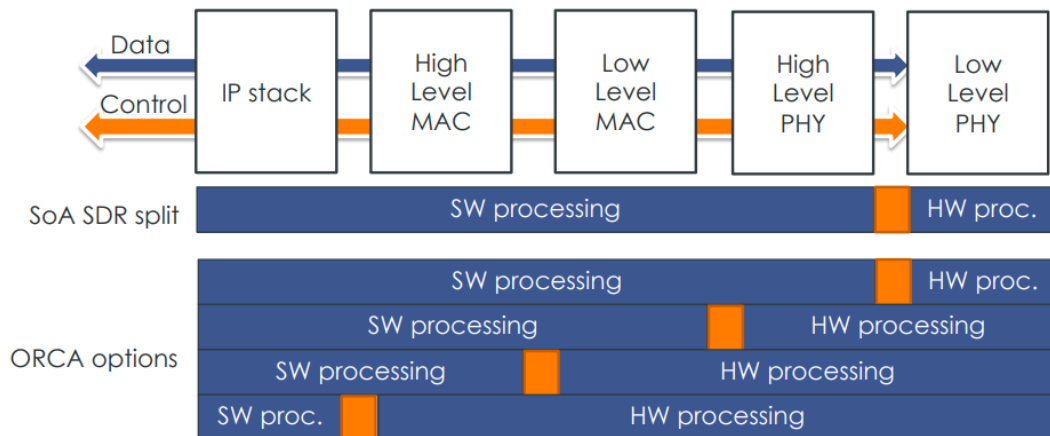
Figure 1.3: Different options for an SDR implementation [1]

2

For 4G/5G standards, several SDR platforms are already available. Examples include *srsLTE* [2] for 4G and *Open Air Interface (OAI)* [3] for 5G. However, SDR has not yet been widely adopted for IEEE802.11 (Wi-Fi). This is mainly due to strict timing requirements defined in the IEEE802.11 standard, as a Short Interframe Spacing (SIFS) of 10 µs/16 µs (2,4 GHz/5 GHz) between the reception of a packet and the transmission of an acknowledgement (ACK) packet is required. This limits the options for an IEEE802.11 SDR implementation, as the host-controlled architecture is no longer possible due to the high latency from the RF frontend.

Here is where the openwifi project [4] enters. Openwifi is an SDR implementation of the IEEE802.11 standard on a Xilinx Zynq System on Chip (SoC). The use of this platform, which tightly couples an FPGA with an ARM processor, allows openwifi to satisfy the SIFS requirement. Additionally, openwifi is an open source project, which allows for open access to the source code for researchers working on projects related to 802.11 networking. Previously, research on 802.11 communication had to make use of existing commercial chips, which has some drawbacks. First of all, by using commercial chips, the research becomes dependent on design choices that were made by the company designing the chip. Secondly, commercial chips don't generally provide access to low level characteristics (think physical layer). For example, Channel State Information (CSI), which is an estimation of the channel conditions, is generally not exposed to the end user. Another example of useful information could be the values used for the contention window (CW) mechanism, as they relate to the latency experienced by the end user.

An example application where openwifi proved to be useful, is the CSI-MURDER project [5] from the Advanced Networking Systems group of the university of Brescia. In this project, openwifi was used to prevent CSI from being used for simultaneous localization and communication. By measuring how CSI amplitude changes over time, it is possible to obtain an estimation of the location of the transmitter. CSI-MURDER makes this estimation impossible by modifying the CSI such that it appears to be randomly generated, thus removing the possibility of unwanted surveillance, while still remaining fully compliant with the Wi-Fi standard. As tinkering with the CSI requires modification of the Wi-Fi frames at the physical layer, this type of application is something which would be very hard to accomplish with commercial chips without access to the source code. Having access to the source code down to the physical layer can thus enable new extensions to existing standards beyond current state-of-the-art.

Currently, the openwifi project supports the 802.11a/g/n standards, with a channel bandwidth of up to 20 MHz. The physical layer is implemented in the FPGA, as is the low MAC layer (Distributed Coordination Function (DCF) for carrier-sense multiple access with collision avoidance (CSMA/CA)). For the upper MAC layer, the mac80211 [6] implementation included in the Linux kernel is used. This has the added benefit that the embedded Linux running on the ARM chip can treat openwifi as a normal Wi-Fi card, and that common user-space management tools can be used, such as iw or wpa_supplicant. Additionally, a lot of parameters can be configured manually, including the SIFS timeout duration and CW related timing.

All physical layers currently supported by openwifi use Orthogonal Frequency Division Multiplexing (OFDM) as the underlying modulation scheme. OFDM has been around for decades, with research dating back to as early as 1966 [7]. The use of OFDM in communication standards has however only been realized in the 90's of the previous century. One of the reasons for this is that an OFDM signal is characterized by a high peak-to-average power ratio (PAPR), which requires the use of sufficiently linear amplifiers, as well as a sufficiently high resolution of the analog-to-digital converter (ADC) / digital-to-analog converter (DAC) used for conversion

to / from the digital domain. Additionally, a fast and efficient implementation of the Fast Fourier Transform (FFT) algorithm is necessary. Both requirements have only been made possible by hardware improvements around that time. The use of OFDM has several advantages. Firstly, due to the use of overlapping (but orthogonal) subcarriers, high spectral efficiency can be obtained compared to traditional Frequency Division Multiplexing (FDM), where an unused guard band is needed between the subcarriers to avoid interference. The use of subcarriers, together with the use of a guard interval, also relates to its robustness against fading in case of multipath propagation. Lastly, compensation for the channel conditions becomes easier, where equalization can be done without the need for convolutions due to the use of the FFT.

Although the openwifi project is already operable with 802.11a/g/n standards compliant devices, one of the features which is still missing in the openwifi project is the use of multiple antennas for communication. Using multiple antennas can be beneficial in the case of challenging multipath environments, as is often the case for indoor deployments of 802.11 systems. This is also the reason why multiple antennas can often be noticed on commercial Wi-Fi access points. The advantages of multi-antenna systems depend on the way the signals coming from the different antennas are used. There are two distinct ways of handling this, which are called spatial diversity and spatial multiplexing.
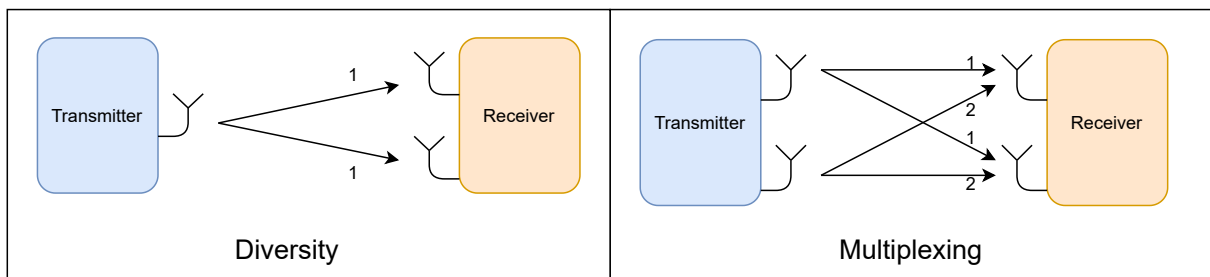
Figure 1.4: Illustration of the difference between spatial diversity and multiplexing

Firstly, spatial diversity is used to improve the quality and reliability of the wireless channel. The principle of spatial diversity is based on the fact that the different antennas all pick up different versions of the same signal. These different versions will also experience different channel conditions, hence the probability that all of the antennas simultaneously experience deep fading is reduced. The effects of multipath propagation can thus be mitigated through the use of spatial diversity. Note that spatial diversity can be employed independently at both the transmitter and the receiver. In other words, spatial diversity can be used at either side of the communication link without the other side's knowledge. The example on figure 1.4 shows the case of receiver diversity, where the receiver can improve its reception by using more than one antenna to receive the same signal from the transmitter.

The second employment of multiple antennas is called spatial multiplexing, or Multiple-Input Multiple-Output (MIMO) as it is more commonly known. The goal of MIMO is now to increase the channel throughput as opposed to the channel reliability. The use of MIMO has been a subject of research for decades, starting in the 70's of the previous century. Its use case originates from the transmission of digital symbols over multiple cables in a cable bundle, where the signals on the different cables are influenced by crosstalk. Later, it was discovered that some of the mathematics could be reused in the case of wireless transmission. The advantage of using MIMO over other techniques, is that the channel throughput can be increased linearly with the number of antennas, without increasing the transmit power or channel bandwidth. In a setting where frequency bands are becoming more and more crowded, MIMO can thus

offer a solution. Still, generally more complex transmitter and receiver implementations are required. Applied to 802.11, MIMO has been incorporated since the 802.11n standard, which was officially released in 2009 and is also known as Wi-Fi 4. However, so-called pre-802.11n products have been released as early as 2005, often using a chipset from Airgo Networks, which included their proprietary MIMO implementation [8]. On figure 1.4, the example shows an example of 2x2 MIMO: the transmitter now sends two different data streams to the receiver, which can use signal processing after the two antennas to distinguish between the separate streams.

Although the advantages of spatial diversity and multiplexing have been proven extensively in theory, research on measurements of practical implementations and a comparison to the theoretical limits are still lacking. With the growing usage of MIMO based techniques to increase throughput in recent new standards, this research becomes increasingly relevant. As an illustration, the 802.11ac standard, which was introduced in 2013 and is also known as Wi-Fi 5, has increased the maximal number of simultaneous MIMO streams from 4 to 8 compared to Wi-Fi 4. Additionally, support for multi-user MIMO (MU-MIMO) was included for downlink communication, which allows multiple devices to receive data from a transmitting device simultaneously. Even more recently, in the 802.11ax standard (Wi-Fi 6), released in February 2021, support for MU-MIMO has been extended to the uplink direction as well. The use of MIMO has also not been limited to 802.11 standards. For instance, the new 5G standard will include support for massive MIMO, which corresponds to the use of a large number of antennas for MIMO. Generally, this implies more then 8 antennas, but numbers up to 256 or even higher might be possible in the future. Massive MIMO is cited as one of the key enabling technologies of 5G [9], as it warrants a high spectral efficiency. In development of the 6G standard, the goal is to extend the massive MIMO concept even further to the cell-free concept, where the location of the antennas is not limited to a single base station, but where these are distributed over a large geographical area.

In the coming chapters, the implementation of spatial diversity and multiplexing on the open-wifi platform will be further discussed. In chapter 2, a theoretical introduction to wireless propagation will be given, as well as an overview of OFDM and why it is such a frequently used technique. A summary of the IEEE 802.11 physical layer is also included in this chapter. In chapter 3, the implementation of spatial diversity and the results obtained from measurements will be discussed. Subsequently, chapter 4 includes the implementation of spatial multiplexing and the corresponding measurements. Finally, chapter 5 lists the conclusions which can be drawn from the thesis, as well as possible future improvements.

Chapter 2

Literature

In this chapter, a theoretical overview of the concepts used in this thesis is given. First, the characteristics of wireless propagation are discussed. Next, the principle behind OFDM will be explained, as well as how OFDM handles the limitations of wireless channels. Throughout the chapter, notes on how these different techniques are used in the various IEEE 802.11 standards are included as well [10].

1 Wireless propagation

In order to design a wireless communication system, it is imperative to have a profound insight in the mechanisms for signal propagation. In general, the quality of any wireless channel is typically [11]:

- site-specific: obstacles surrounding the antennas can reflect or scatter the radio signal.
- location-dependent: changing the position of transmission and/or reception antennas causes a rapid variation of the signal level. This phenomenon is called fading.
- time-dependent: for a fixed site and fixed antenna locations, the signal level can still vary over time. This is due to the fact that scatterers influencing the propagation can move around. The wireless channel is said to be time-variant.

Since it is impossible to fully describe a realistic propagation environment with all scatterers together with their movements over time, the characteristics of a wireless channel are mostly described by using statistics. It is then up to the designer to create a system which can handle the rapid signal variations.

As to the different effects that can influence the signal level at the receiver, the first effect is called path loss. This effect is dictated by the propagation of electromagnetic waves through space and possible absorption losses when propagating through lossy media. Path loss dictates the mean signal level which is to be expected at a certain distance from the transmitter, and can be represented by the so-called path loss exponent. This value indicates how quickly the mean signal level decays when increasing the distance from the transmitter. Values between 2 and 6 can be expected, with a value of 2 corresponding to free-space transmission, whereas higher values can occur in environments with lots of reflections, such as in dense urban environments.

Path loss can explain the fact that the average signal level follows a log-linear model with respect to the distance from the transmitter. The path loss exponent can then be obtained
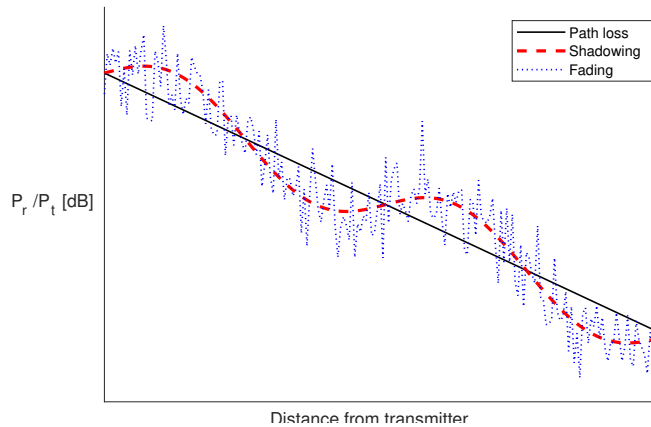
Figure 2.1: Illustration of the received signal power P_r vs. distance from the transmitter

by fitting a straight line through the measured data. However, when considering the average signal strength over a circle with a radius of about 10 wavelengths, additional fluctuations can be seen that are not explained by path loss. These fluctuations are caused by shadowing: this typically occurs when large obstructions, such as buildings or hills, obstruct some of the signal paths between transmitter and receiver at certain positions. In the assumption of multipath transmission, where a lot of different reflections arrive at the receiver, it can be shown that the received signal level shows a log-normal distribution. Shadowing is thus caused by the fact that at some locations, less (or less strong) multipath components are received, which leads to a change in the received signal level compared to the values expected from path loss.

An illustration of the influence of path loss and shadowing on the received signal level is shown on figure 2.1. As can be seen, there is also a third effect that plays a role, which is called fading. Fading is caused by constructive or destructive interference between different multipath components when moving the transmitter over distances of half a wavelength. As such, the relative phase of the different multipath components plays a role: destructive interference will occur when these components show a phase difference of π rad. It can be shown that the signal level follows a Ricean distribution in case a LOS path is available, or a Rayleigh distribution otherwise [11]. The Rayleigh distribution is obtained in the assumption that there are lots of scatterers present in the environment, such that the received signal consists of multiple multipath components.

Next to shadowing and fading, the presence of multipath transmission and a dynamic environment with moving scatterers and/or receivers also causes variations of the signal level over time and frequency. In case the scatterers and/or receiver are moving, signals reflecting from different moving objects will experience different Doppler shifts: the centre frequency of each of the multipath components will be perceived differently by the receiver due to its motion relative to the transmitter. The maximal Doppler spread $f_{D,m}$ which can occur is related to the coherence time τ_c of the channel: this is the time duration over which the channels impulse response can be considered constant. Additionally, due to the different multipath components each arriving at slightly different times, the channel is characterized by a delay spread τ_{ds}. The result of this difference in arrival times is that the channel becomes frequency-selective: different frequency components of the signal will experience different channel conditions. A measure for indicating the frequency selectivity of the channel is given by the coherence bandwidth B_c: this value indicates the maximal frequency range over which the channel can be

considered flat, and thus that near frequency components will experience the same fading. The relation between the different values is approximately given by equation (2.1).

$$f_{D,m} \approx \frac{1}{\tau_c} \qquad\qquad \tau_{ds} \approx \frac{1}{B_c} \qquad\qquad (2.1)$$

In order to counter the effects introduced by the wireless channel, several methods are possible. Most communication systems will typically include automatic gain control (AGC) in the receiver path to oppose the rapid signal level variations caused by fading. However, accounting for the frequency-selectivity and time-varying nature of the channel is more difficult. One of the ways to deal with this is Orthogonal Frequency Division Multiplexing (OFDM), which will be explained in the next section.

(a) Frequency flat channel

(b) Frequency selective channel
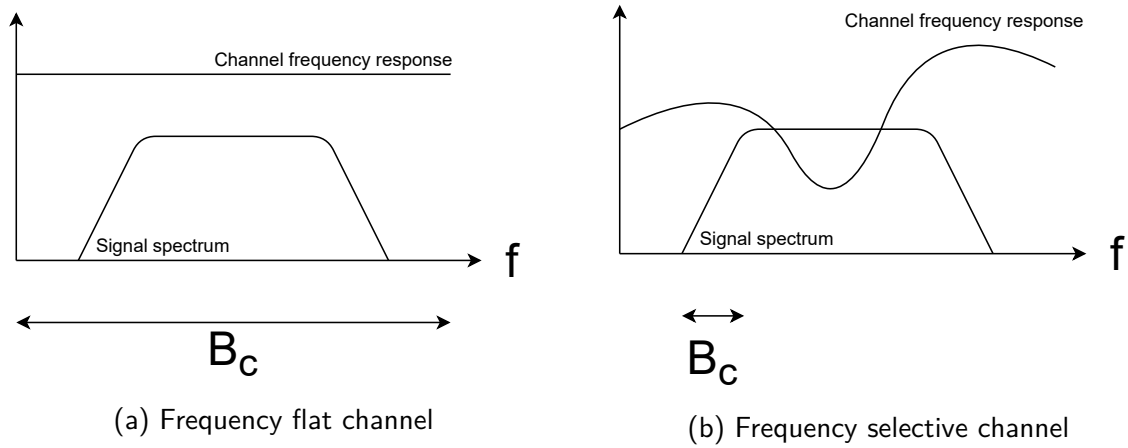
Figure 2.2: Channel types

To get an idea of the order of magnitude of these phenomenon, some examples can be considered. Considering a case where different multipath components arrive at a receiver communicating around a centre frequency f_c of 5 GHz, the maximal Doppler spread is given by $f_{D,m} = 2v\frac{f_c}{c}$, where v represents the relative speed difference between the receiver and the reflecting environment. In case this speed is equal to 10 km/h / 100 km/h, a corresponding channel coherence time of around 10 ms/1 ms is found: the channel can be considered constant for this duration. Additionally, some values concerning the frequency-selective nature of the channel can be considered. The maximal delay spread τ_{ds} varies from around 10 ns in indoor environments with lots of nearby scatterers, to 10 μs in hilly terrains, where the objects reflecting the incoming signals can be found further away. This corresponds to a channel coherence bandwidth B_c of respectively 100 MHz and 100 kHz.

2 OFDM

One of the ways to deal with the frequency selective nature of the channel is to use OFDM. The principle behind OFDM is to convert a sequence of data symbols from a single high-rate sequence to many low-rate sequences which are modulated on different subcarriers and transmitted in parallel. Since the subcarriers divide the total bandwidth in many smaller ranges, each subcarrier can now be treated as a separate, frequency flat channel. This is due to the fact that the subcarrier bandwidth can be smaller than the coherence bandwidth. Additionally, the system becomes more robust against intersymbol interference (ISI), as the symbol duration for each of the subcarriers becomes longer. Even though the used subcarriers are overlapping in the frequency domain, this is not a problem due to the orthogonality of the subcarriers. This is illustrated on figure 2.3. In what follows, a theoretical explanation of OFDM will be given [12]. The explanation will be given in the digital domain, as this is how OFDM is used on an FPGA.
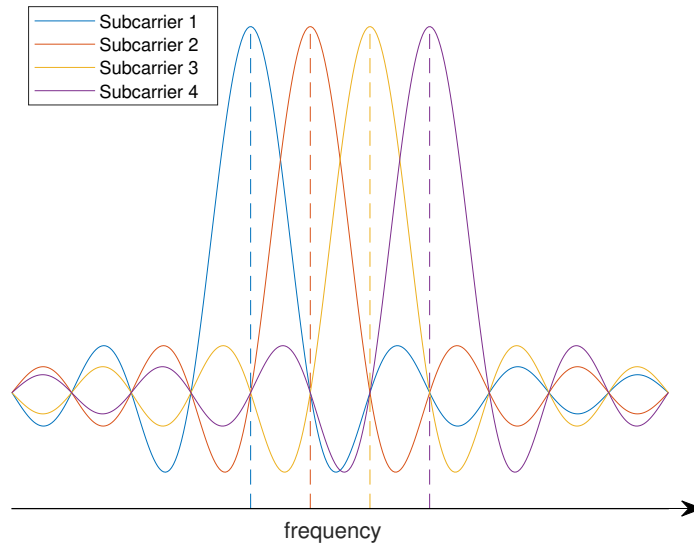
Figure 2.3: Illustration of the orthogonality of the OFDM subcarriers

2.1 Transmitter and receiver implementation

The structure of a general OFDM transmitter is given on figure 2.4. The transmitter starts from a symbol sequence $a(k)$ of a certain constellation (e.g. BPSK or a form of QAM). Next, a serial to parallel conversion is applied, using the notation $a(iN + n) = a_n(i)$ $(0 \leq n < N)$. Here, N represents the total number of subcarriers. $a_n(i)$ is then the symbol on the n-th subcarrier from the i-th block. Then, the IDFT is applied to the N symbols from the current block: this results in N outputs $[x_0(i), x_1(i), \cdots, x_{N-1}(i)]$. A cyclic prefix (CP) is inserted in the output before the parallel to serial conversion. The CP is obtained by reusing the latest ν outputs of the IDFT: outputs $[x_{N-\nu}(i), \cdots, x_{N-1}(i)]$ are inserted in front of the other IDFT outputs. Note that the cyclic prefix is called the guard interval (GI) in IEEE 802.11 terminology. Finally, a parallel to serial conversion is applied and the samples are sent through a transmit filter to obtain the full baseband signal, which will later be upconverted to the carrier frequency before the wireless transmission occurs.

The receiver starts from the baseband signal obtained after downconverting the received signal. Next, a receive filter is applied to the baseband signal, which can be applied either in the analog
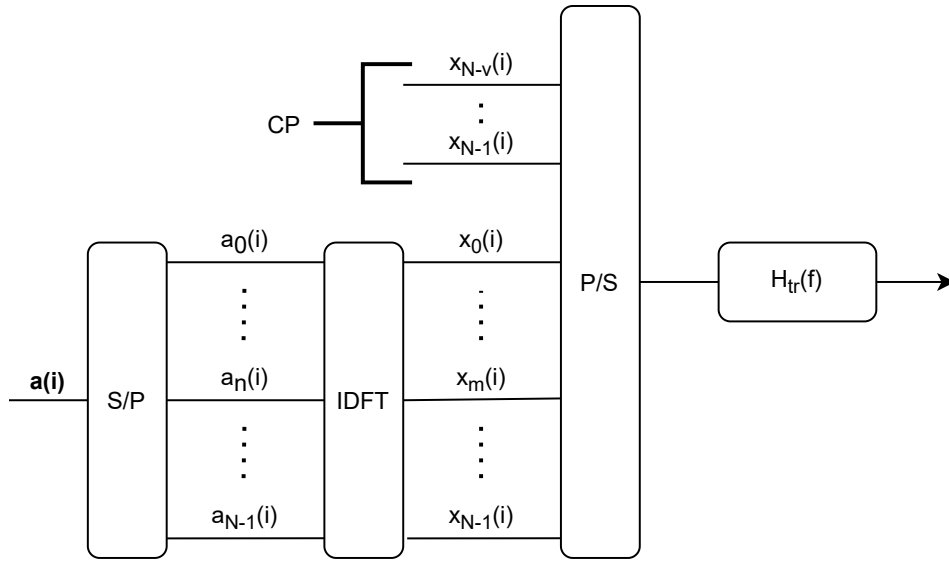
Figure 2.4: Structure of an OFDM transmitter

or in the digital domain. Afterwards, a serial to parallel conversion is applied. The receiver can discard the part of the current block that constitutes the CP, and applies the Discrete Fourier Transform (DFT) to the remaining part of the current block. Finally, the output of the receiver can be used to estimate the original symbols $a(k)$ after a parallel to serial conversion.
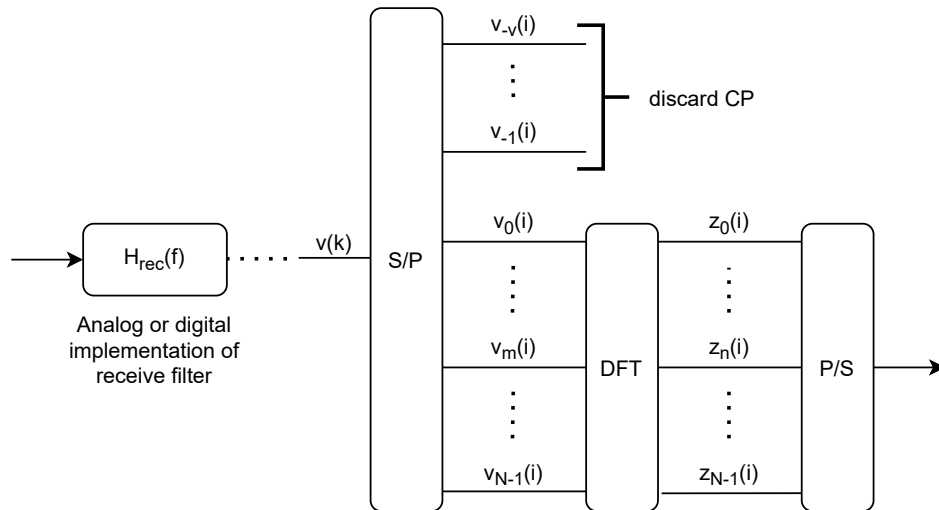
Figure 2.5: Structure of an OFDM receiver

From these diagrams, it might seem as if the cyclic prefix is redundant, as it is discarded by the receiver anyway. There are however two reasons for insertion of the cyclic prefix. Firstly, the cyclic prefix makes it such that a linear convolution with the OFDM transmitter output is equivalent to a circular convolution, as long as the length of the sequence with which the convolution is executed is smaller than or equal to the length of the cyclic prefix. This equivalence is illustrated on figure 2.6. As will become clear in the next section, this is a very useful property.

Secondly, introduction of the cyclic prefix avoids the occurrence of inter-block interference (IBI). This is very important in case of multipath transmission, where multiple delayed copies of the same signal are received due to reflections in the environment. An example situation
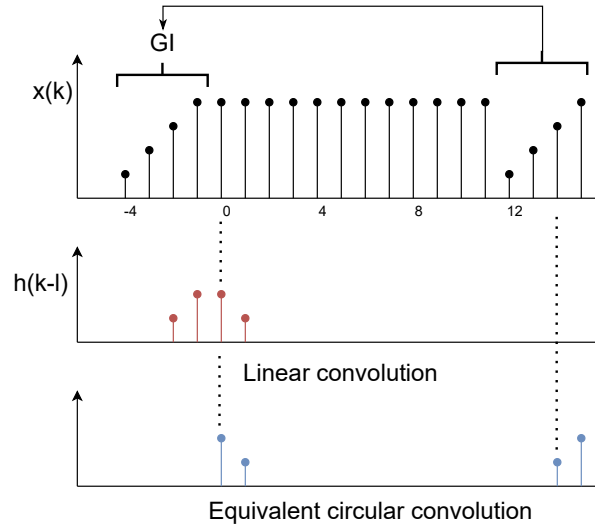
Figure 2.6: Example showing the equivalence of linear convolution to circular convolution due to the introduction of a GI

is depicted on figure 2.7. In case no guard interval is used, the delayed signal of the first symbol overlaps with the start of the second symbol. This means that IBI will occur, as there is interference due to the overlap of two adjacent symbols. In case a guard interval is introduced, IBI is avoided, as now the overlap between adjacent symbols falls entirely within the guard interval.

(a) Without guard interval   (b) With guard interval
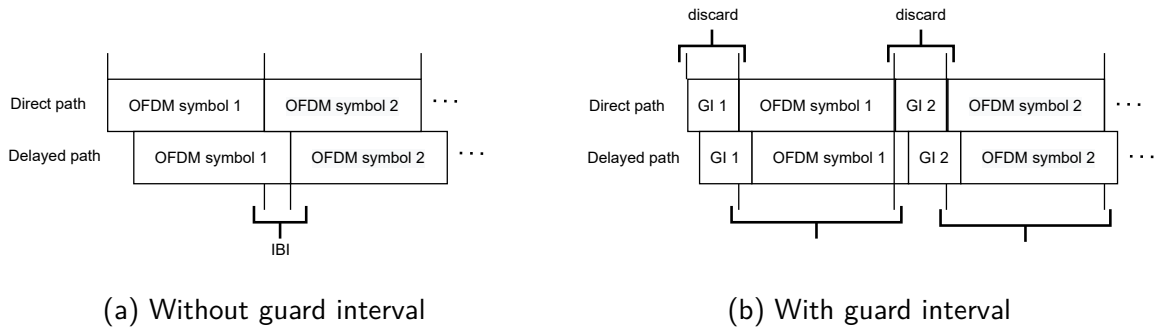
Figure 2.7: Importance of the guard interval in case of multipath transmission

Note that introduction of the guard interval does entail a reduction in channel throughput, as part of the total transmission time is no longer used to send data. In order to avoid unnecessary use of the channel for transmission of the GI, the GI duration should be equal to the maximal delay spread of the multipath components, as this is the minimal value necessary to avoid IBI. As an example, IEEE 802.11a specifies a GI duration equal to 800 ns, whereas IEEE 802.11n introduced the so-called short GI of 400 ns. Introduction of the short guard interval allows IEEE 802.11n to operate at higher throughputs, but has as a disadvantage that performance in environments with a large delay spread will be reduced due to the occurrence of IBI.

2.2 Influence of different non-idealities

The system as represented in the previous section is the basic principle behind OFDM and did not take into account the fact that the wireless channel and analog electronics introduce

several effects that need to be addressed. These effects are listed below:

1. frequency selective channel
2. carrier frequency offset (CFO)
3. sampling frequency offset (SFO)

The first effect is due to the combined influence of the transmit filter $H_{tr}(f)$, the receive filter $H_{rec}(f)$ and the channel transfer function $H_{ch}(f)$. Note that the channel is assumed to be time invariant. This assumption is valid in case the channel coherence time is larger than the duration of an OFDM symbol. Representing the combination of all three filters by the transfer function $H(f)$ and its corresponding impulse response by $h(k)$, the relation between the output of an OFDM transmitter $x(k)$ and the input of the OFDM receiver is given by a convolution: $v(k) = (x * h)(k)$. Due to the introduction of the cyclic prefix, this linear convolution is equivalent to a circular convolution, as long as the CP is chosen long enough: ν has to be at least equal or larger than the total channel memory, which is given by the number of k for which $h(k) \neq 0$. This equivalence is already explained in the previous section and illustrated on figure 2.6. Next, the receiver can apply the DFT to the samples $v(k)$, after removing the cyclic prefix. The property that the DFT of a circular convolution leads to a multiplication of the transfer functions in the frequency domain is then used to obtain the resulting output. Following the notation of figure 2.5, this output is equal to $[H_0 z_0(i), H_1 z_1(i), \cdots, H_{N-1} z_{N-1}(i)]$. Here, the sequence $[H_0, H_1, \cdots, H_{N-1}]$ corresponds to the DFT of the total impulse response $h(k)$.

From this result, it can be seen that correcting for the channel conditions (channel equalization) becomes relatively simple, as equalization can be done on a subcarrier basis. The symbol on each subcarrier can be derived as simple as dividing the output of DFT by the corresponding channel coefficient H_n. In literature, this approach is known as zero forcing (ZF) equalisation, as the interference from the channel is fully removed. However, a disadvantage of the ZF approach is that any noise on the symbol is ignored. As an example, consider the case where H_n starts becoming very small: dividing by a small number will boost any noise that was already present on the symbol. As a consequence, ZF can actually cause a decrease in the signal to noise ratio (SNR). Another well-known approach which solves this problem is called minimun mean square error (MMSE) equalisation. In this case, the aim is no longer to fully remove the influence of the channel, but rather to minimize the combined influence of channel and noise. In MMSE, some assumptions need to be made about the noise, which is typically assumed to be Gaussian. It can be shown that MMSE equalisation performs better than simple ZF equalisation under different channel conditions [13]. However, the MMSE approach is more complex, as an estimate for the noise statistics has to be made. Note that for both approaches, knowledge of the channel coefficients is necessary in order to apply the correct equalisation. In the openwifi receiver, ZF equalisation is used.

The second non-ideality which needs to be accounted for, is the carrier frequency offset (CFO). This effect occurs due to an offset in the received carrier frequency and the local oscillator (LO) used in the receiver. The offset can be caused due to a mismatch between the transmitter's and receiver's LO, and additionally by the Doppler effect in case the transmitter or receiver is moving. In the receiver, this effect causes a phase rotation of the incoming samples. In order to compensate for the CFO, an additional phase rotation thus needs to be applied to the incoming I/Q samples before they are processed by the DFT. In IEEE 802.11n, a maximum centre frequency offset of 20 ppm is specified [10, p.2307]. This thus leads to a maximal CFO of 40 ppm between transmitter and receiver.

The final non-ideality which can occur is called the sampling frequency offset. This effect is caused by a sampling offset as compared to the samples that were generated at the transmitter. An illustration of the effect is given on figure 2.8. SFO introduces a phase rotation after the DFT. This is shown in equation (2.2), where $w(k) = v((k+\epsilon)T_s)$ represents the signal sampled with an offset ϵT_s. This effect can be countered by applying the correct phase shift after the DFT.

$$
\begin{aligned}
W(m) &= \sum_k w(k) \exp\left(-j2\pi\frac{km}{N}\right) \\
&= \sum_k \sum_l x(l)h((k+\epsilon-l)T_s) \exp\left(-j2\pi\frac{km}{N}\right) \\
&= \sum_k \sum_l x(l)h((k+\epsilon-l)T_s) \exp\left(-j2\pi\frac{(k+\epsilon-l)m}{N}\right) \exp\left(-j2\pi\frac{lm}{N}\right) \exp\left(j2\pi\frac{\epsilon m}{N}\right) \\
&= X(m)H(m) \underbrace{\exp\left(j2\pi\frac{\epsilon m}{N}\right)}_{\text{additional phase term}}
\end{aligned}
$$

$$(2.2)$$
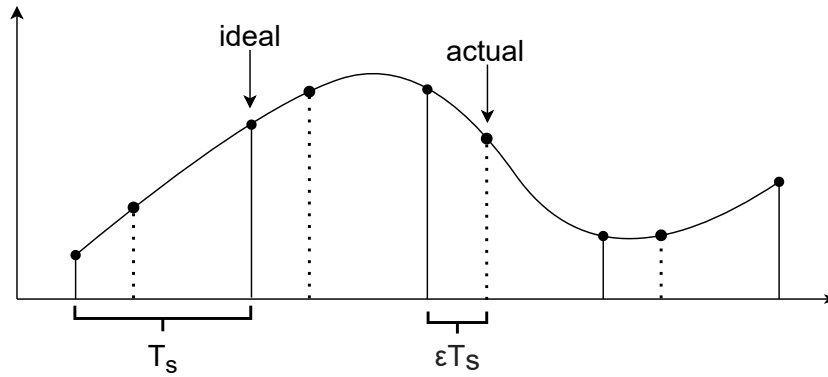
Figure 2.8: Illustration of the sampling frequency offset

2.3 OFDM in IEEE802.11

In IEEE802.11, OFDM is the most frequently used modulation technique over the different standard versions. Exceptions are 802.11 legacy and 802.11b, which use direct-sequence spread spectrum (DSSS). In 802.11a/g/n, the number of OFDM subcarriers equals 64 in case a channel width of 20 MHz is used. However, as is shown on figure 2.9, not all subcarriers are used to transmit data. In standard 802.11a/g, only the 52 inner subcarriers are used, whereas in HT mode, which was introduced in 802.11n, 56 subcarriers are used. The reason that the outer subcarriers are not used is to avoid out-of-band emissions, such as not to interfere with other nearby channels. Additionally, some of the subcarriers are also reserved to transmit pilot symbols, which are used to keep track of the SFO for each OFDM symbol.

In order for the receiver to apply the corrections for the effects introduced by the channel and the different frequency offsets, IEEE 802.11 specifies a short (L-STF) and a long (L-LTF) preamble. The structure of these preambles is given in figure 2.10. The short preamble is
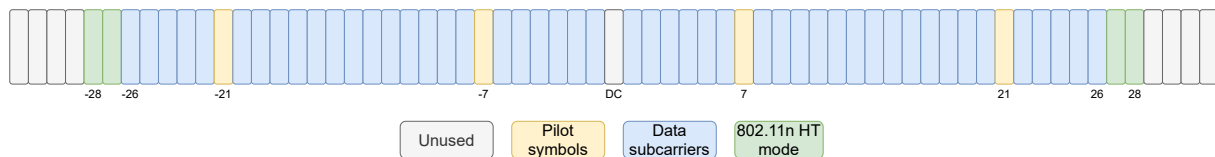
Figure 2.9: OFDM subcarriers in IEEE802.11 a/g/n

constructed from the IDFT of a sequence where 1 out of 4 subcarriers are BPSK modulated and the remaining is set to 0. Execution of the IDFT then results in a sequence of 64 samples, which consists of a repetition of the same 16 samples for 4 times. These 16 samples are repeated 10 times in order to obtain the short preamble [10, p.2360]. The goal of the short preamble is to allow the receiver to detect the start of a transmission, as well as to allow the AGC to converge to the mean signal level. Additionally, the short preamble can be used to estimate the CFO, by measuring the phase difference between the repetitions of these 16 samples, as this represents the accumulated CFO over the short preamble. The long preamble can be used to gain knowledge about the channel coefficients, which is necessary in order for the receiver to apply equalisation correctly. This is done by sending two OFDM symbols with known values, such that the receiver can deduct the channel coefficients. Furthermore, the long preamble is used for synchronization, such that the receiver knows where each OFDM symbol starts. This can be done by calculating the cross-correlation between received IQ samples and the known L-LTF samples, as the peaks in the correlation indicate the starting position of the first and the second OFDM symbol.
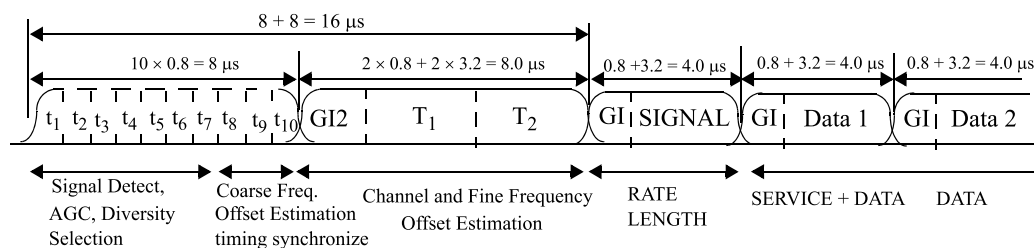
Figure 2.10: OFDM training structure in IEEE 802.11 [10, p.2289]

Note that the estimation of the channel coefficients is thus only done at the start of a full packet, which consists of multiple OFDM symbols. In order for this estimation to be valid for the whole packet duration, the coherence time of the channel should be larger than the packet duration. From the section on wireless propagation, it was shown that the minimal coherence time at a centre frequency of 5 GHz was between 1 and 10 ms. However, the maximal packet duration in 802.11n HT mode is equal to 5484 µs [10, p.662]. Consequently, in dynamic environments with a large Doppler spread, the estimation of the channel coefficients could be invalid at the end of the packet, since the channel has changed in the meantime. In fact, in 802.11ax the midamble was introduced specifically to counter channels with a larger Doppler spread. Due to a periodic repetition of a training sequence inside the physical layer packet (PPDU), the estimate of the channel coefficients can then be adjusted during packet reception.

As for the validity of the equalization of the subcarriers, the coherence bandwidth of the channel also plays a role. Since equalisation of the subcarriers assumes that each of the subcarriers is subject to frequency-flat fading, the width of a subcarrier should be smaller than the coherence bandwidth of the channel. Again, it was found in the previous section that the

coherence bandwidth is typically between 100 kHz and 100 MHz. However, up until 802.11n, the subcarrier spacing is equal to 312,5 kHz [10, p.2354]. Thus, in environments with a large delay spread, the channel equalisation can become invalid, as the subcarriers are now also subject to frequency-selective fading. In 802.11ax, the subcarrier spacing has been reduced from 312,5 kHz to 78,125 kHz, which should make the new standard more robust against larger delay spreads.

3

Spatial Diversity

Spatial diversity is a very useful technique to increase the robustness of any wireless communication system by using multiple antennas. Many of these techniques do however require adaptations on both the receiver and transmitter side, which makes detailed specification in standards compulsory. An example of such a technique is Space-Time Block Code (STBC), which has been added to the Wi-Fi standard as from 802.11n. In STBC, the values from neighbouring OFDM symbols are combined in different ways and sent over multiple antennas. The receiver then uses the information available from the different transmission times in order to discern the original OFDM symbols. For this reason, STBC requires modifications at both ends of the wireless link. Furthermore, these modifications are not limited to the physical layer only, as additional signalling is required in the MAC layer to convey to other nodes which types of STBC are supported. For these reasons, the interest of this thesis goes more towards diversity approaches that only require modifications on one side of the communication link. At the receiver side, these techniques include different forms of combining, where the signals coming from the different antennas are used to combat fading. These techniques will be further explored in section 1. At the transmitter side, the focus will be on cyclic shift diversity (CSD), which will be discussed in section 2.

1 Receiver diversity

1.1 Theory

For the explanation of the theory behind spatial diversity, a situation will be considered using OFDM communication as described in chapter 2. Starting from a symbol sequence $a(k)$ with energy $E_s = E[|a(k)|^2]$, the corresponding OFDM symbols are obtained as on figure 2.4, resulting in the sequence $x(i)$. Considering the case where multiple diversity paths (i.e. multiple antennas) are available to a receiver, the received signal on diversity path j is given by the convolution of the channel (and receive and transmit filters) with $x(i)$.

$$v_j(k) = (h_j * x)(k) + n_j(k) = \sum_i h_j(i)x(k-i) + n_j(k) \tag{3.1}$$

Note that the channel impulse response h_j is different for each of the different diversity paths. The channel is also assumed to be time invariant (see chapter 2): the impulse responses $h_j(k)$ do not vary for the duration of the transmission. Additionally, a noise term n_j is included in

the expression as well. The noise is modelled as additive white gaussian noise (AWGN): n_j is a sequence of circularly symmetric complex normal variables with zero mean and autocorrelation $\sigma_j \delta(k)$. The noise on the different diversity paths are assumed to be statistically independent.

At the receiver, the operation described on figure 2.5 can be applied to obtain the sequence $z_j(l + iN)$ for each of the different diversity paths, where N represents the used DFT length. As explained in chapter 2, due to the introduction and subsequent removal of the guard interval, the convolution between the channel impulse response and the sequence $x(i)$ can be considered as a circular convolution (assuming that the guard interval is long enough), hence equation (3.2) is obtained.

$$z_j(l + iN) = H_j(i)a(l + iN) + n_{f,j}(l + iN) \tag{3.2}$$

Here, $H_j(i)$ represents the channel coefficient on diversity path j and subcarrier i. $n_{f,j}(i)$ is obtained as the DFT of $n_j(k)$ and is thus still a sequence of circularly symmetric random variables, but the variance increases from σ_j to $\sigma_{f,j} = \sqrt{N}\sigma_j$. After calculating the DFT, the receiver can then account for the channel conditions on each diversity path. From chapter 2, we recall that in IEEE802.11 the channel coefficients are obtained from the long preamble. Assuming that the coefficients $H_j(i)$ are thus perfectly estimated by the receiver, equation (3.3) can then be applied for each diversity path.

$$\begin{aligned} \hat{a}_j(l + iN) &= \frac{H_j^*(i)}{|H_j(i)|^2} z_j(l + iN) \\ &= a(l + iN) + n_{a,j}(l + iN) \end{aligned} \tag{3.3}$$

The new noise term in equation (3.3) now has a variance of $\sigma_{f,j}/|H_j(i)|$. The obtained signal to noise ratio (SNR) on each diversity path j and each subcarrier i depends on the channel conditions on that subcarrier: in case $|H_j(i)|$ is small, the SNR will be reduced. This is due to the assumption of white noise: since the noise power is constant over all frequencies, a decrease in $|H_j(i)|$ will lead to a decrease in the SNR.

$$\text{SNR}_{j,i} = \frac{|H_j(i)|^2 E_s}{\sigma_{f,j}^2} \tag{3.4}$$

In order for the receiver to decode the transmission, $\hat{a}_j(k)$ can be used to find the original symbol sequence $a(k)$. Now, there are different options available for the receiver on how to use the different diversity paths. These methods will be introduced below in order of descending optimality. The first method is called maximum ratio combining. In this case, the receiver scales the contributions from the available diversity paths according to $\text{SNR}_{j,i}$: this implies that paths with a better SNR will contribute more to the final symbol $\hat{a}(l + iN)$. This is expressed in equation (3.5).

$$\hat{a}(l + iN) = \frac{\sum_j \text{SNR}_{j,i} \, \hat{a}_j(l + iN)}{\sum_j \text{SNR}_{j,i}} \tag{3.5}$$

The SNR over all diversity paths is now obtained as the sum of all paths, i.e. $\text{SNR}_i = \sum_j \text{SNR}_{j,i}$. Maximal ratio combining is the most optimal method: it can be shown that no other method will result in a higher SNR.

The second method is called equal gain combining. The diversity paths are now directly added together without additional scaling. This is shown on equation (3.6). Here, an additional

scaling factor D is necessary such that $E[|\hat{a}(k)|^2] = E_s$, where D represents the total number of diversity paths available to the receiver.

$$\hat{a}(l + iN) = \frac{1}{D} \sum_j \hat{a}_j(l + iN) \tag{3.6}$$

The resulting SNR is given in equation (3.7). Comparing this result to the maximal ratio combining scheme, the SNR obtained with the equal gain combining scheme will always be smaller than or equal to the SNR in case of maximal ratio combining. Equality is achieved whenever the SNR on all paths is equal: in this case maximal ratio combining is equivalent to equal gain combining.

$$\text{SNR}_i = \frac{DE_s}{\sum_j \frac{\sigma_{f,j}^2}{|H_j(i)|^2}} \tag{3.7}$$

The final method is called selection combining. Instead of using all diversity paths at the same time, now only one path is used at a time. The used path corresponds to the path with the best channel conditions over all subcarriers. This is expressed in equation (3.8). The SNR in case of selection combining is simply equal to $\text{SNR}_{j,max}(i)$: the conditions of the best available diversity path determines the overall channel.

$$\hat{a}(l + iN) = \hat{a}_{j_{max}}(l + iN) \quad \text{with } j_{max} = \text{argmax}_j \left(\sum_i \text{SNR}_j(i) \right) \tag{3.8}$$

The disadvantage of the selection combining scheme is that it does not use the array gain which could be provided by using the signal power from multiple antennas. Array gain is achieved due to the fact that the received power will increase together with the number of antennas that are used. This is also reflected in the SNR: the signal power in the selection combining scheme does not increase.

The power of diversity combining lies in the fact that the effects of fading can be mitigated. In the case of maximal ratio combining, this can be proven by looking at the variance of the SNR. To simplify the problem, the assumption will be made that the noise on all diversity paths follows the same distribution, which implies that $\sigma_{f,j} = \sigma_f$ for all j. The noise on different diversity paths remains uncorrelated. Additionally, the statistics of the channel are assumed to be the same on the different diversity paths. Again, the channels on the different diversity paths remain uncorrelated. Applying these assumptions results in the expressions in table 3.9.

	Single antenna	D antennas	
$E\left[\text{SNR}_i\right] \propto$	$E\left[|H(i)|^2\right]$	$D \cdot E\left[|H(i)|^2\right]$	(3.9)
$\text{Var}\left[\text{SNR}_i\right] \propto$	$\text{Var}\left[|H(i)|^2\right]$	$D \cdot \text{Var}\left[|H(i)|^2\right]$	

The expected SNR increases linearly with the number of diversity paths, which is achieved due to the array gain. Additionally, the variance increases as well. However, since the mean SNR has increased, a better measure for the variation of the SNR is given by the relative standard deviation, which is equal to the standard deviation divided by the mean. Applied to the values from table 3.9, the relative standard deviation decreases with a factor of $1/\sqrt{D}$ compared to the single antenna use case. For the equal gain and selection combining schemes, the expressions for the variance are more involved. However, also there the variation of the SNR will be reduced, albeit to a lesser extent than with maximal ratio combining.

In terms of implementation complexity, maximal ratio combining is the most difficult to achieve. This is due to the fact that the receiver needs to know the SNR on each of the different diversity paths, and then rotate and scale the incoming symbols from all paths before adding them together. Equal gain combining reduces the complexity by removing the need to estimate the SNR. In selection combining, complexity is reduced even further due to the fact that now only a single receive path is used at a given time. This implies that the operations required to obtain $\hat{a}_j$ from z_j (DFT and channel correction) need to be performed only for the best diversity path instead of for all of them. The receiver does still need to find a way to estimate the SNR on all paths.

1.2 Implementation

For implementation on the openwifi platform, the choice was made to go with the equal gain combining scheme. This is due to the fact that this removes the need for SNR estimation at the receiver. Although this is possible to do in IEEE802.11 systems by using the long preamble, the added complexity on the FPGA is not proportional to the gain that is to be expected. As shown in [14], the performance of equal gain combining under Rayleigh fading conditions is very close to the performance of maximal ratio combining, and as such the additional gain of maximal ratio combining does not warrant the added complexity.

To move on to the implementation of equal gain combining, first the openwifi design needs to be introduced. An overview of the complete openwifi system is given on figure 3.1. The FPGA module relevant to the implementation of receiver diversity is the *openofdm_rx* block. This block takes in the baseband I/Q samples from the RF frontend after passing through a digital down-converter in the *rx_intf* module. These samples are coming in at a speed of 20 MHz, which corresponds to a new sample every 50 ns. After decoding, the bits are transferred to the *rx_intf* module, which will transfer these bits to the ARM chip.
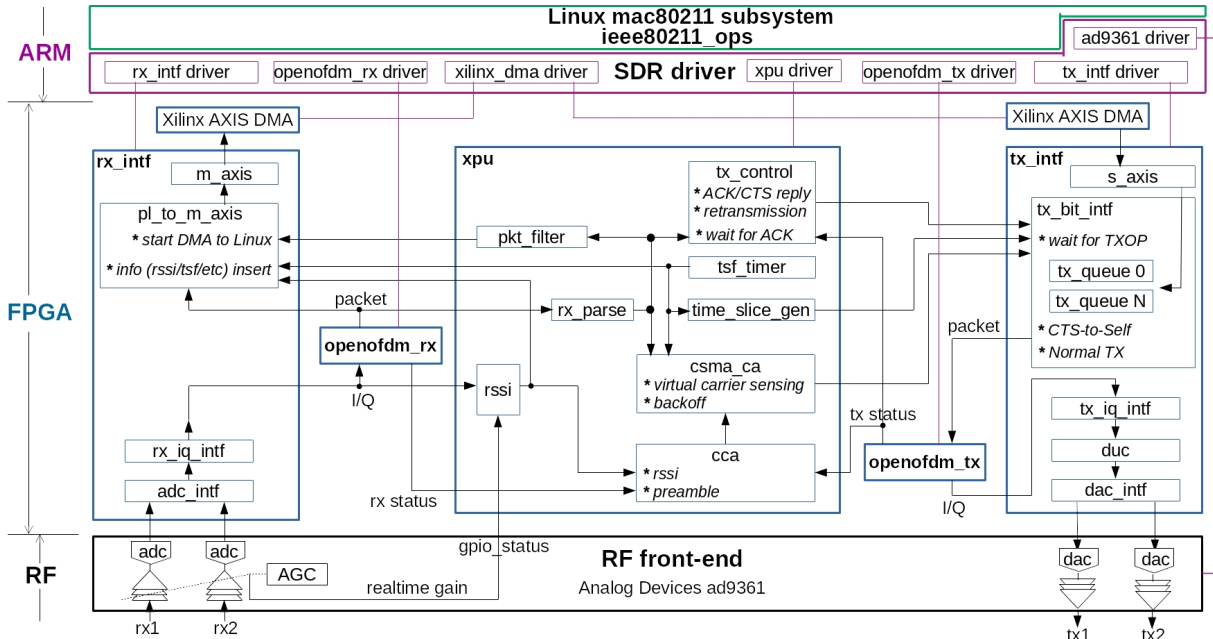

Figure 3.1: Openwifi design overview [4]

In the original *openofdm_rx* module, the structure from figure 3.2 is used in order to obtain the packet information from the incoming I/Q samples. Here, the following modules are present:
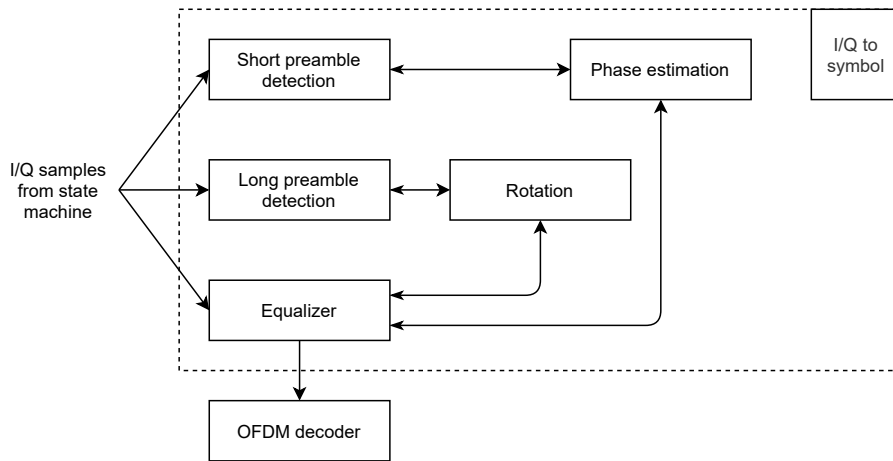
Figure 3.2: Overview of the original openwifi receiver

Short preamble detection This module is used to detect the start of a transmission, which is indicated by the short preamble as given on figure 2.10. Additionally, this module uses the short preamble to get an estimate of the CFO. This can be accomplished by calculating the accumulated phase increase over 16 samples, as the short preamble is a periodic sequence which repeats after 800 ns.

Long preamble detection In order for the receiver to accurately remove the guard interval, the position of the start of each OFDM symbol needs to be known. By calculating the cross correlation over the two long preamble symbols, this synchronization can be achieved. Additionally, this module is responsible for the guard interval removal and subsequent DFT to go from the time to the frequency domain. In order to do this, first a rotation is applied to the incoming I/Q samples to account for the CFO, where the estimation made during the short preamble can be used.

Equalizer This module contains the necessary corrections that need to be applied in the frequency domain in order to obtain the data symbols. Here, the channel coefficients estimated during the long preamble are used to perform the equalization. Additionally, the phase estimation module used during the CFO estimation in the short preamble is now reused to estimate the SFO by means of the pilot symbols inside each OFDM symbol. The rotation module from the long preamble can be reused to rotate the symbols according to the estimated SFO.

OFDM decoder The decoder is responsible for converting the incoming data symbols to data bits. The module performs the conversion from coded bits to data bits using a Viterbi decoder, and subsequently performs deinterleaving and descrambling to obtain the full PSDU. The logic to decode the signal fields inside the PPDU is also included in this module: this is needed to derive the transmit rate and other options that need to be known by the receiver in order to successfully decode a packet.

On figure 3.2, the modules encircled by the dotted line correspond to the modules that need to be duplicated for the equal gain combining implementation. The duplicated modules are jointly referred to as "I/Q to symbol" block. This modified design is shown on figure 3.3. The symbols from each antenna are now saved in FIFO queues before being added together. The FIFO queues are required since the symbols coming from both antennas are not necessarily synchronized. By only reading from the FIFOs when both of the queues are not empty, the

Figure 3.3: Modified receiver with equal gain combining

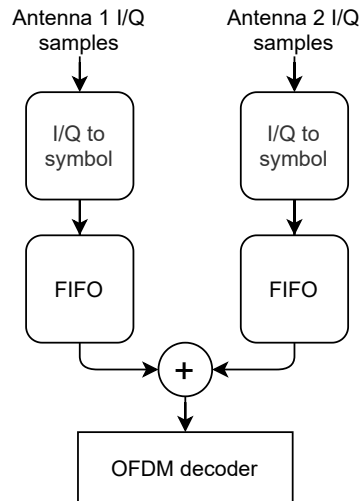addition of both symbols can be applied correctly. Additionally, it could happen that only a single antenna can detect a signal. This case is handled by starting to read from the queues just before one of the queues is full: in this case, no combining is applied, but the symbols from a single antenna are used for the remaining duration of the PPDU.

In order to determine the size of the FIFO queues, it is important to know what the difference in timing between both antennas can be. The cause of this difference in timing is related to the accuracy of the long preamble synchronization, which determines the start of the OFDM symbols. In the final design, it was decided to support a maximal difference in the estimated start of the OFDM symbols on both antennas of 3 I/Q samples. At a sampling rate of 20 MHz, this comes down to a maximal time difference between both antennas of 150 ns. In order to translate this timing to the FIFO size, it is important to realize that the clock used by the receiver runs at a speed of 200 MHz. This implies that the 'I/Q to symbol' identifier on figure 3.3 will output data symbols at an interval of 5 ns. Thus, in order to cover the maximal 150 ns difference between the two antennas, it is necessary to have a FIFO size of at least $150/5 = 30$ samples. However, two additional clock cycles are needed in order to start reading from the queues before they start overflowing: this is due to the fact that the signal indicating that the FIFO is almost full requires one clock cycle to reach the state machine controlling the combining operation. The other clock cycle is then required for the read enable signal coming from this state machine to reach one or both FIFO queues. Thus, both FIFO queues require a size of 32 I/Q samples.

1.3 Measurements

The setup used to measure the performance of the combining implementation is depicted on figure 3.4. The openwifi SDR board is connected with coax cables to a commercial off-the-shelf (COTS) device. Since all boards used by openwifi have separate transmit and receive antennas, a combiner is necessary in front of the COTS device, as it only has a single antenna port for both transmission and reception. The hardware used to run openwifi is the ADRV9361-Z7035 module on the ADRV1CRR-FMC carrier board, both from Analog Devices. In the openwifi reception path, two configurable attenuators are included to emulate different fading scenarios. Additionally, to exclude the influence of external interference and other Wi-Fi equipment operating in nearby frequency channels, the openwifi board and COTS device are

each isolated in a Qosmotec shielding box.
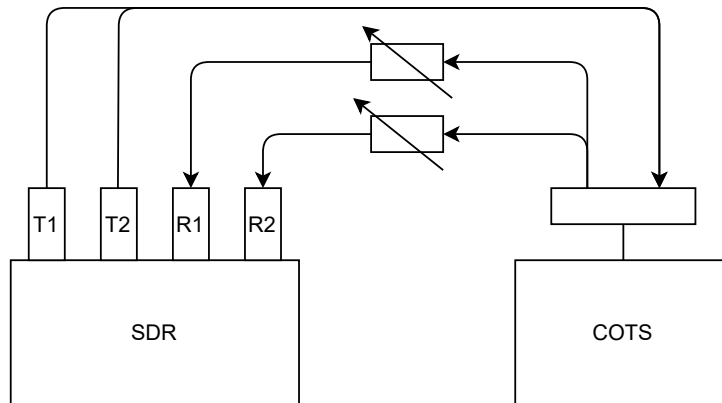
Figure 3.4: Lab measurement setup

For the measurements, the openwifi board is used as an access point (AP), and the COTS device acts as a client connecting to the openwifi board. Then, for different settings of the attenuation on both receive ports, the transmit rate which is most frequently used by the COTS device is measured at the openwifi board. Since Linux includes a mechanism for automatic rate control (called minstrel), the transmit rate of the COTS device will change according to the used attenuation values. To verify the functionality of the test setup, first the RSSI was measured at one of the SDR's receive ports when changing the attenuation. The result of this measurement is shown on figure 3.5. It was found that the relation between the attenuation and the measured RSSI was only linear until a certain point, where the RSSI converges to a value of around $-78\,$dBm. The non-linearity is due to the fact that only RF power splitters are used at the testbed instead of circulators. This means that any signal transmitted by the COTS device will arrive at both the transmit and receive ports of the openwifi board. The lower bound on the RSSI that can be achieved is thus caused by leakage on the SDR board from the transmit to the receive ports.
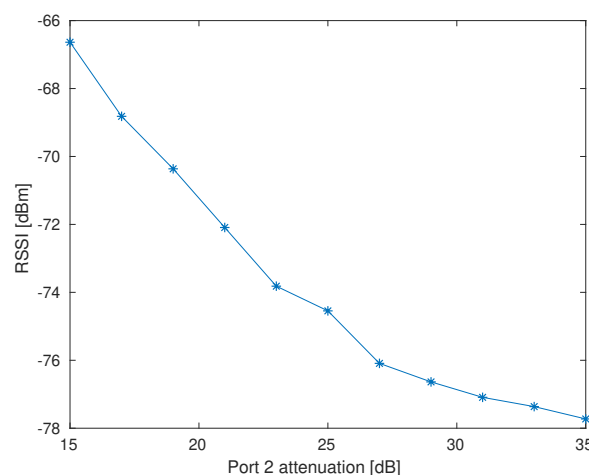
Figure 3.5: RSSI at openwifi

Fortunately, the linear region of the RSSI versus attenuation curve is sufficient to trigger the minstrel algorithm to switch between certain transmit rates. Minstrel does not rely on the measured RSSI directly, but uses a metric based on the probability of a successful transmission

together with the measured throughput to determine which transmission rate should be used [15]. But since the transmission success probability of higher rates will decrease as the received power drops, minstrel should adapt the used transmission rate whenever the attenuation is increased. The result of the measurement is shown on figure 3.6. For the measurements where no combining is used, only the attenuation on port 2 influences the transmission rate, since only a single antenna is used. When using both antennas in the combining mode, the attenuation on both antennas starts to play a role. Now, a higher transmission rate can be used by the COTS device even if a large attenuation is present on one of the two antennas.

In a less controlled environment, the used transmission rates will depend on the environment and fading statistics. However, by using spatial diversity, higher transmission rates can be supported, due to the expectation that simultaneous fading at both antennas is less likely to occur than fading at only a single antenna. In the case of fading at a single antenna, the other antenna can still receive the signal and a dropped packet can be avoided.

(a) Without combining   (b) With combining
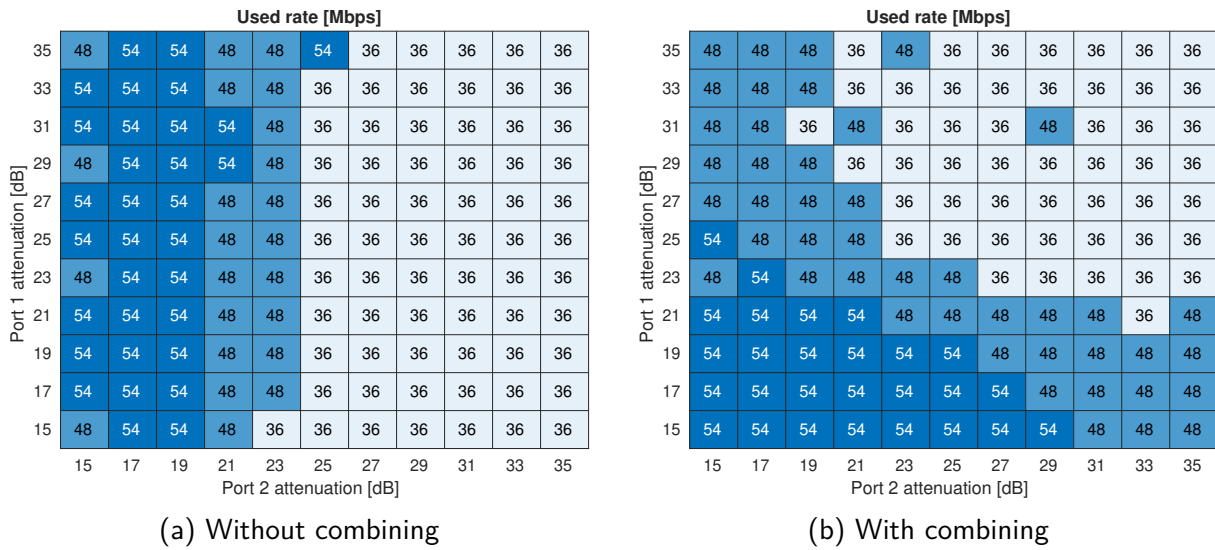
Figure 3.6: Diversity combining measurement results

2 Transmission diversity

2.1 Theory
....

In chapter 2, it was shown that OFDM based communication systems can still be reliable in multipath conditions, due to the introduction of the GI and the use of channel equalisation. Actually, the performance of such a system can benefit from the presence a large number of (preferably uncorrelated) multipath components . A simple technique to increase the number of multipath components at the receiver would be to transmit a delayed version of the signal at each of the antennas. This technique is known as Delay Diversity, and was originally introduced by Wittneben in 1993 [16]. By introducing a larger delay spread at the receiver, the channel will become more frequency-selective and the coherence bandwidth will decrease, which implies that the fading experienced by adjacent subcarriers will be less correlated. However, the limitation of this technique is that it tries to mimic a physical multipath component, and as such will result in a larger delay spread at the receiver. Applied to OFDM based systems, the maximal delay that can be applied is consequently limited by the length of the GI. In case the artificial delay introduced at one of the antennas results in a too large delay spread at the receiver, this will unavoidably lead to IBI, as explained in chapter 2.

In order to circumvent this disadvantage, Kaiser originally proposed a different diversity scheme for OFDM called phase diversity (PD) [17]. The baseband signal for each antenna is now obtained by multiplying the symbols before execution of the IDFT with a linearly increasing phase factor. The advantage over delay diversity is now that additional frequency-selectivity is introduced without increasing the delay spread. In [18], Kaiser indicated that the PD scheme can also be implemented in the time domain, rather than multiplying by a linearly increasing phase in the frequency domain. This is due to the equivalence relation between a shift in time and a phase factor brought by the DFT. In case the PD scheme is implemented in the time domain, it is better known as cyclic delay diversity (CDD) or cyclic shift diversity (CSD). Both approaches are illustrated on figure 3.7 in case two transmit antennas are used.

(a) Phase diversity (b) Cyclic shift diversity
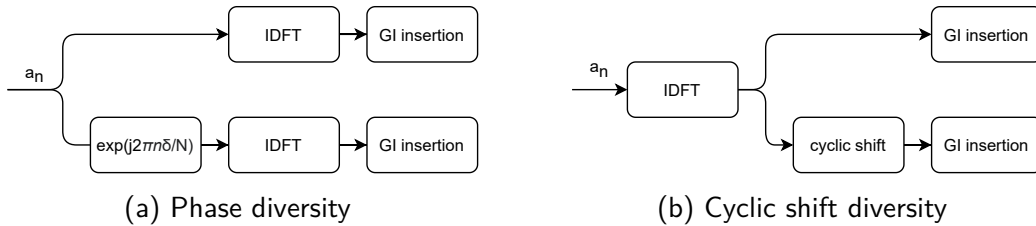
Figure 3.7: Two equivalent transmit diversity schemes

There is still a distinction between the two methods, despite the fact that they are both different implementations of the same diversity scheme. The first difference has to do with the complexity of implementation. As can be seen on figure 3.7, implementation of PD requires that a separate IDFT calculation is performed for each antenna. This makes the PD scheme more complex, as CSD only requires a single IDFT for all antennas. Additionally, the complexity of a phase multiplication also exceeds that of a cyclic shift in time. Another difference between both approaches lies in the frequency selectivity which can be obtained. Since the cyclic shift is an operation which is performed in the digital domain, it should be taken into account that the cyclic shift can only occur in discrete steps. This limitation does not apply to PD, as any arbitrary phase factor can be chosen here. Thus, the CSD scheme is less complex, but also less configurable.

As an example to show the influence of the cyclic shift, the artificial channel created by the introduction of CSD can be considered. Equation (3.10) shows the impulse response introduced by applying CSD, which results in a corresponding DFT as shown in equation (3.11). Here, N_{ant} is equal to the number of antennas used for transmission, N_{CS} is equal to the number of samples that are cyclically shifted, and N equals the DFT length. The factor $1/\sqrt{N_{ant}}$ is included to make sure the total transmitted power stays the same when increasing the number of transmit antennas.

$$h_{CSD}(m) = \frac{1}{\sqrt{N_{ant}}} \left[\delta(m) + \delta(m - N_{CS}) + \delta(m - 2N_{CS}) + \cdots \right. $$
$$\left. + \delta(m - N_{ant}N_{CS}) \right] \tag{3.10}$$

$$H_{CSD}(k) = \frac{1}{\sqrt{N_{ant}}} \left[1 + \exp\left(-j2\pi k \frac{N_{CS}}{N}\right) + \exp\left(-j2\pi k \frac{2N_{CS}}{N}\right) + \cdots \right.$$
$$\left. + \exp\left(-j2\pi k \frac{N_{ant}N_{CS}}{N}\right) \right] \tag{3.11}$$

After transmission, the receiver will calculate the DFT and correct for the channel conditions as explained in section 2. However, due to the introduction of the cyclic shift, the channel as measured by the receiver will be equal to $H_{CSD}(k)H_{ch}(k)$. $H_{CSD}(k)$ is shown on figure 3.8 in the case of $N_{ant} = 2$, $N_{CS} = 4$ and $N = 64$. As can be seen, the application of CSD will introduce additional frequency selectivity. From equation (3.4), we recall that the SNR on each subcarrier is determined by the corresponding channel coefficient. Although the SNR on some of the subcarriers is reduced, the gain on other subcarriers can compensate for this loss in case sufficient coding and interleaving is applied.
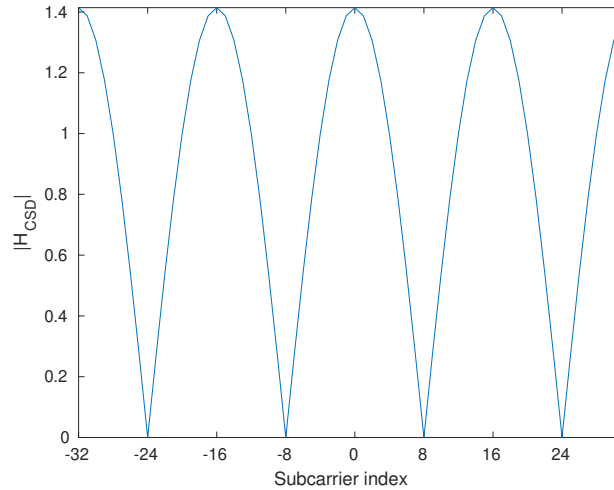
Figure 3.8: $|H_{CSD}|$ for $N_{ant} = 2$, $N_{CS} = 4$ and $N = 64$

2.2 Implementation

For the implementation on the openwifi platform, the choice was made to go for the CSD scheme in order to achieve transmission diversity. Since the sample rate at the IDFT calculation is equal to 20 MHz, this implies that the cyclic shift which can be applied will be a multiple of 50 ns. The operation required to perform CSD is very simple in OFDM. As the name states,

all that is required is a cyclical shift of the samples coming from the output of the IDFT, before the guard interval is introduced. The required cyclic shift operation is illustrated on figure 3.9.
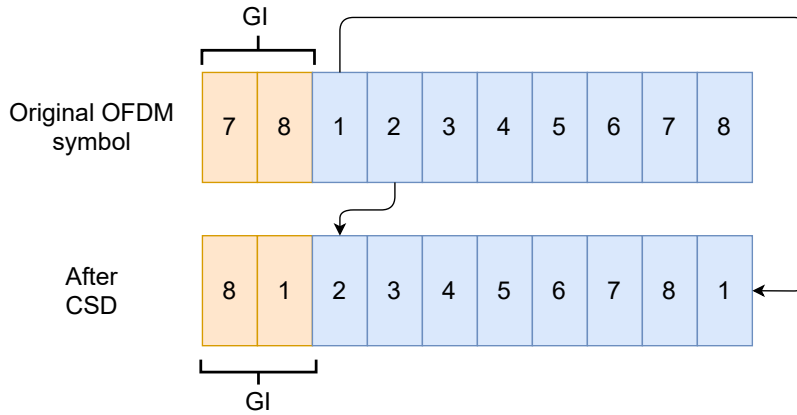
Figure 3.9: Illustration of the cyclic shift applied to a single OFDM symbol

In order to include the CSD operation on the openwifi board, two modules from the FPGA design from figure 3.1 need to be modified. First, the *openofdm_tx* block needs to be modified to double the amount of output I/Q samples. Additionally, the second I/Q pair needs to be cyclically shifted compared to the first I/Q pair. Secondly, the *tx_intf* block needs to be adapted to accept the doubled amount of I/Q samples. Finally, some modifications to the ARM driver are required as well in order to activate the second transmit antenna on the RF frontend.

Figure 3.10 shows part of the unmodified *openofdm_tx* module relevant to the application of CSD. The output of the IDFT is saved in two separate FIFO queues: one for the packet I/Q samples and another for the CP samples. The FIFOs are enabled by a state machine at the correct time, such that the right output samples are selected. The final output of the module is assembled from the two FIFO queues and several ROM modules, which contain the different types of preambles.
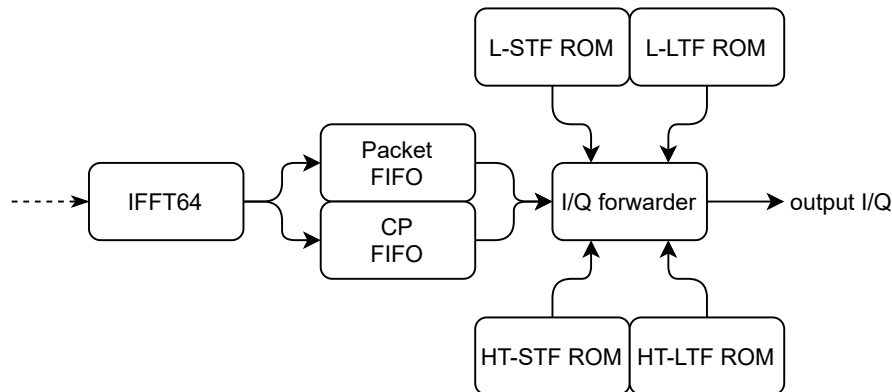
Figure 3.10: Overview of part of the unmodified *openofdm_tx* module

In order to create the cyclically shifted version of each OFDM symbol, three additional FIFO queues are needed. Two of these queues are used to hold the CP and packet IQ samples for the second antenna. An auxiliary FIFO queue is included to perform the cyclic shift: this FIFO holds the first samples from each OFDM symbol which have to be moved to the end of the

current symbol (see figure 3.9). Also, additional logic is required to select the correct input from either the IDFT output or the CSD FIFO. The modified design is shown on figure 3.11.
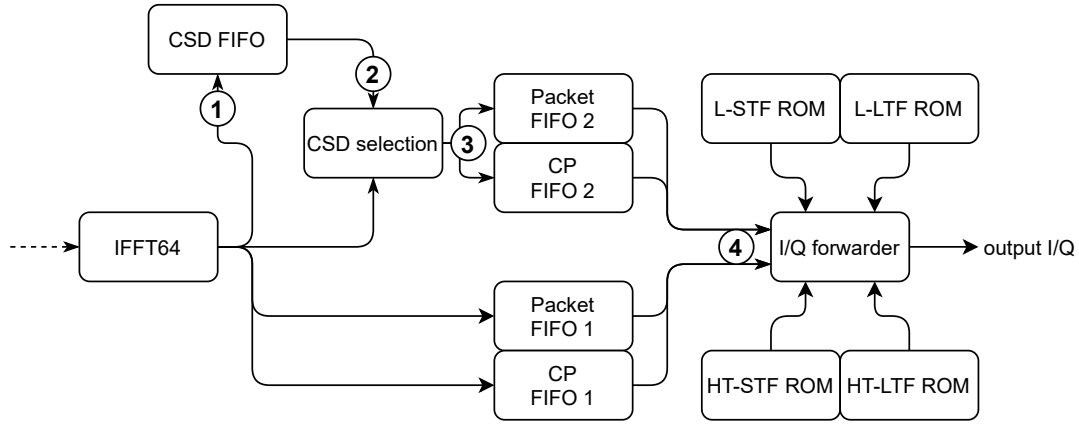
Figure 3.11: Overview of part of the modified *openofdm_tx* module

The timing of the CSD FIFO write enable signal needs to be aligned with the first IDFT samples. The design has been made such that the number of samples used for the cyclic shift N_{CS} is configurable. In the 802.11 standard, it is specified that the value of the cyclic delay should be equal to -200 ns or -400 ns in case two antennas are used [10, p.2360, 2363]. At a sampling rate of 20 MHz, this corresponds to $N_{CS} = 4/N_{CS} = 8$. However, other values can be used as well since the receiver does not need to know the value of N_{CS} to decode the signal. On figure 3.12a, the timing of the write enable signal is shown, corresponding to connection ① on figure 3.11. As can be seen, the first $N_{CS} = 4$ I/Q samples from the OFDM symbol are written to the CSD FIFO. As for connection ② on figure 3.11, the CSD FIFO's read enable signal needs to be activated one clock cycle before the start of the next OFDM symbol to account for the one clock cycle read delay. The first N_{CS} samples from the current OFDM symbol are thus saved in the CSD FIFO and output when the IDFT block outputs the first N_{CS} samples of the next OFDM symbol.

(a) write enable timing ①

(b) read enable timing ②
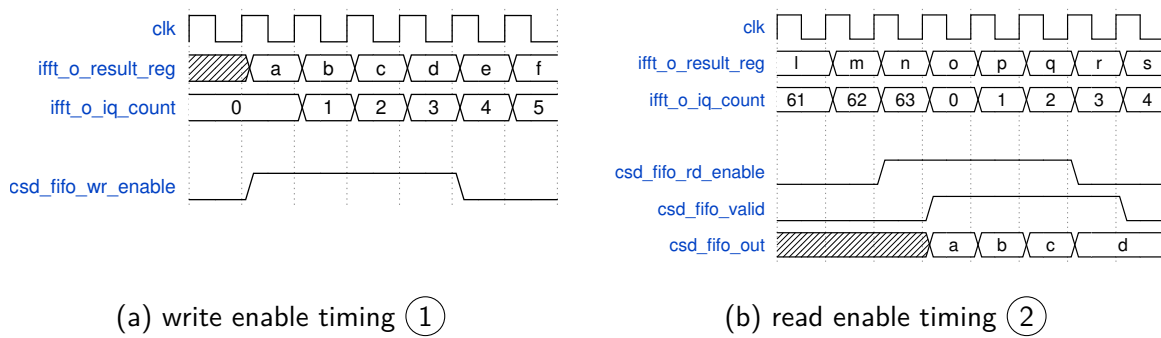
Figure 3.12: CSD FIFO timing

The input of the packet and CP FIFOs corresponds to connection ④ on figure 3.11 and is shown on figure 3.13. As can be seen, the input data of the FIFO queue of the second antenna is delayed with N_{CS} samples with respect to the first antenna due to the introduction of the cyclic shift. The timing difference between both antennas is later eliminated at connection ④ by only reading from the FIFO queues when the queues from both antennas indicate that they are ready. The additional delay of N_{CS} samples introduced at connection ④ does not influence the transmission timing, due to the fact that the preambles need to be sent before the

samples from the packet and CP FIFOs can be read. Additionally, the openofdm_tx module is running at a clock speed of 200 MHz, which is 10 times as fast as the 20 MHz speed at which the baseband samples are consumed by the RF frontend. For that reason, the SIFS timing is not influenced.
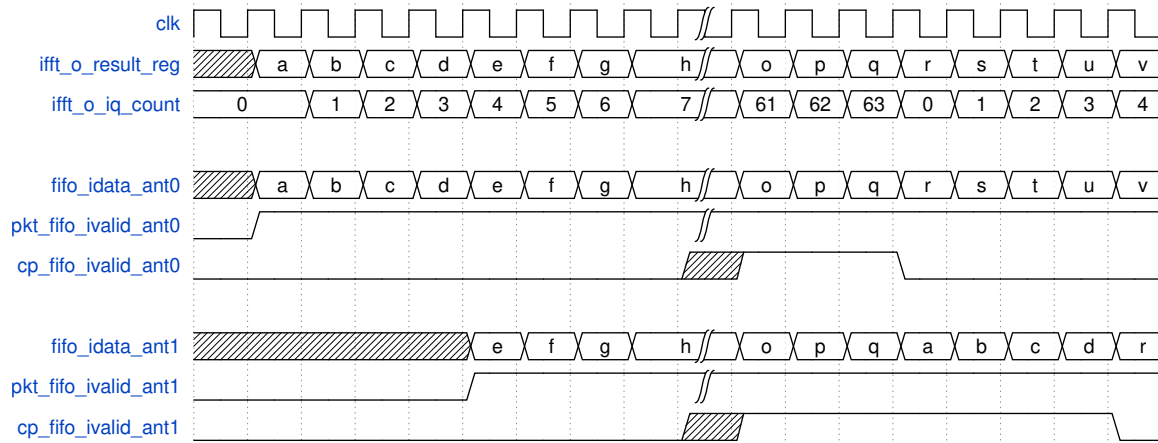
Figure 3.13: Packet and CP FIFO input signalling ③

2.3 Measurements

In order to verify the working of the CSD implementation, the measurement setup from section 1.3 was reused. Since CSD influences the channel characteristics at the receiver, both the RSSI and CSI were measured at the COTS device. The CSI measurement is made possible by a feature called 'spectral scan' included in the drivers used on the COTS device [19].
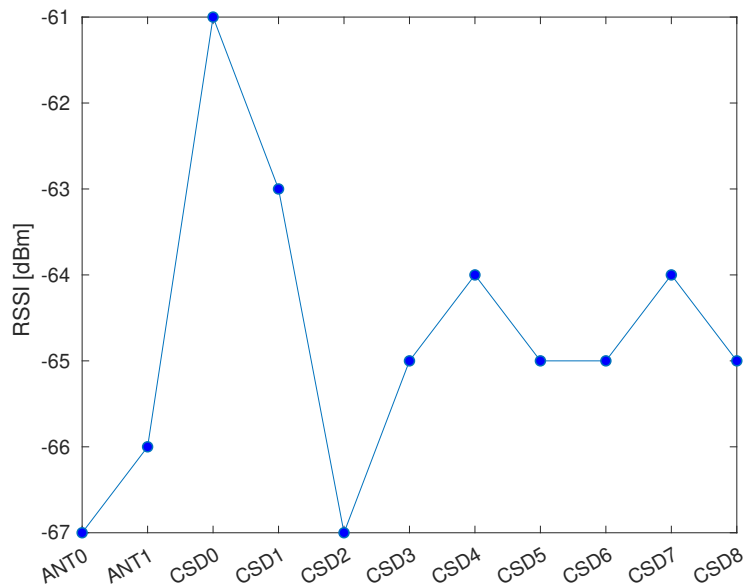
Figure 3.14: RSSI measurement on the testbed

28

On figure 3.14, the measured RSSI is shown for different situations. The indices on the figure should be interpreted as follows:

ANT0 and ANT1 These measurements describe the situation where only a single antenna is used. They have been added as a reference.

CSD0 In this situation both antennas are used without CSD. This results in a gain of 6 dBm compared to the case where only a single antenna is used. This gain is explained by the coherence between the signals on the two antennas.

CSDX In these situations, two antennas are used with a cyclical shift of X samples, which corresponds to a cyclical time difference between both antennas of $X \cdot 50$ ns. It can be seen that on average, application of CSD results in a gain of around 3dBm.

Based on figure 3.14 alone, the benefit of CSD may not be clear and requires additional explanation. The disadvantage of coherent signals on both antennas is that the resulting signal at the receiver can be subject to either constructive or destructive interference. In case of the testbed, the measured RSSI is the result of constructive interference at the COTS device. However, in real world applications, the occurrence of either type of interference is much more random, and also depends on the location of the receiver compared to the transmit antennas. Additionally, in case destructive interference occurs, it can happen that no signal is found at the receiver at all. By introducing CSD, the coherence relation between both antennas is destroyed, which also removes the occurrence of constructive and destructive interference. This will lead to a smaller increase in RSSI, which is however more stable and does not depend on the location of the receiver. For that reason, it is also stated in the IEEE 802.11 standard that application of CSD prevents "unintentional beamforming" [10, p.2360].

As an additional remark, note that for correctly evaluating the influence of the CSD approach, actually the transmit power on each antenna should have been halved, as now figure 3.14 also shows the influence of doubling the transmit power. Also, the maximally transmitted power has to be smaller than the values specified by the relevant regulatory authorities. In Europe, this is handled by the European Telecommunications Standards Institute (ETSI). For operation in the relevant 5 GHz band, a minimum value of 20 dBm EIRP is specified [20]. However, for application on the openwifi platform, the additional 3 dB is welcome, as the total transmit power is always below 20 dBm, even when using both antennas. This is due to the fact that the RF frontend used by openwifi is not optimized for a single frequency band, but rather for wideband application, as is desirable for a SDR.

On figure 3.15, the resulting CSI measured at the COTS device is shown. The additional frequency selectivity introduced by the application of CSD is to be expected, as explained under section 2.1. Referring back to equation (3.4), the fluctuation in channel gain will also lead to a fluctuation in the SNR of the different subcarriers. This in turn implies that the bit error rate on some subcarriers will increase and decrease on others. However, due to sufficient coding and interleaving, this will not influence the overall throughput.
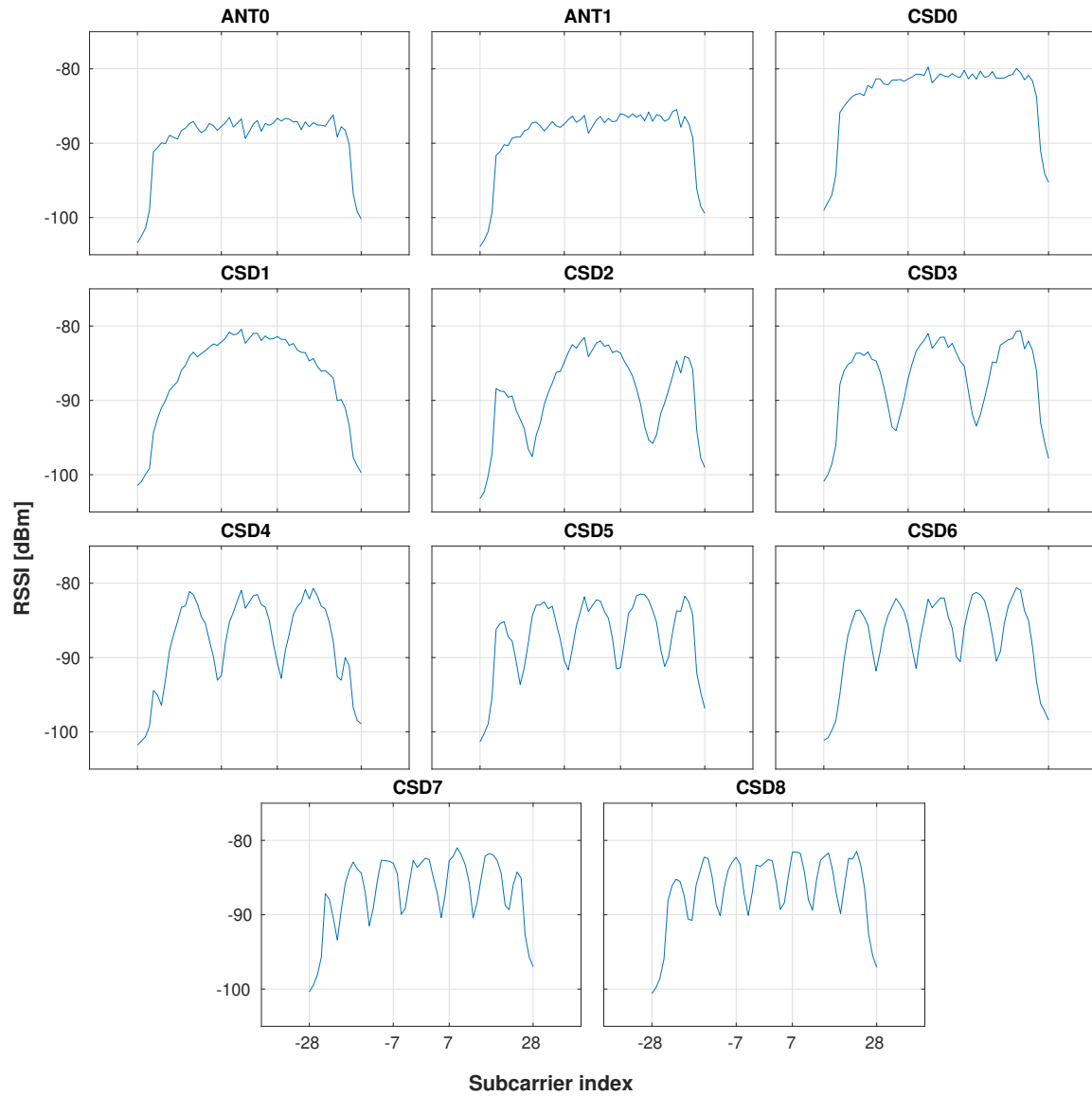
Figure 3.15: CSI measurement on the testbed

4

Spatial multiplexing

In recent years, spatial multiplexing or MIMO has been one of the main techniques used to increase the throughput in wireless communication standards. Applied to IEEE802.11, MIMO has been present since Wi-Fi 4 (IEEE802.11n). Compared to the chapter on spatial diversity, this chapter will need to adhere more to the standard in order to be interoperable with other systems using MIMO, as modifications at both the receiver and transmitter are now required.

1 Theory

Traditionally, the upper limit on throughput in wireless communication was considered to be determined by Shannon's Law [21], which is repeated in equation (4.1). Here, the channel capacity C [bits/s] is determined by the bandwidth W [Hz] and the signal to noise ratio.

$$C = W \log_2 \left(1 + \text{SNR}\right) \tag{4.1}$$

In order to increase the channel capacity, either the bandwidth or the SNR had to be increased. However, there are limitations on the improvements that can be obtained this way. By moving to larger bandwidths, electronics that can work over a large range of frequencies are required. Additionally, larger bandwidths can not always be obtained in licensed bands if the neighbouring bands are already occupied. As for the SNR, either the transmit power can be increased or the noise level at the receiver can be reduced. For battery operated devices, increasing the transmit power is not always feasible. Reducing noise levels also corresponds to better electronic designs. Furthermore, the channel capacity depends logarithmically on the SNR, so doubling the transmit power will not result in an equally proportional gain in channel capacity.

By using MIMO, these limitations can be circumvented. MIMO is possible in case more than one antenna is present at both the transmitter and the receiver. In this case, the upper limit on the channel capacity increases linearly with the number of antennas that are used. For the analysis, we will again start from a sequence of symbols $a_j(k)$ with symbol energy $E\left[|a_j(k)|^2\right]$. However, each antenna now has its own sequence of symbols, as indicated by the index j. For each antenna, the transmitter can calculate $x_j(k)$ as on figure 2.4, and transmit $x_j(k)$ on antenna j. At the receiver, the signals from the transmitters antennas are added together at each of the receivers antennas. This is depicted on figure 4.1 in the case of a 2×2 configuration.
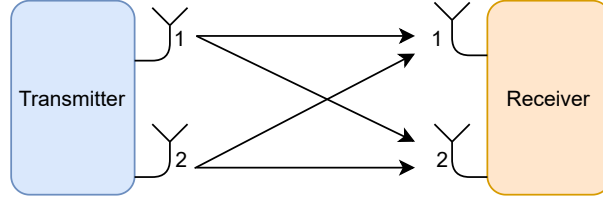
Figure 4.1: Antenna numbering in case of 2×2 MIMO

The resulting signal at receiver antenna i is given by equation (4.2). Here, h_{ij} represents the impulse response of the channel (and receive and transmit filter) between transmit antenna j and receive antenna i. Note that all of the transmit antennas thus contribute to the received signal on a single antenna.

$$v_i(k) = \sum_j (h_{ij} * x_j)(k) \tag{4.2}$$

The receiver can again apply the procedure from figure 2.5 to go from v_i to z_i. The expression for z_i is given in equation (4.3). Compared to the case where no MIMO is used, retrieving a_j is more difficult, since now the symbols from all transmit antennas contribute to z_i. By moving to matrix notation, it can be seen that inversion of the channel matrix $\boldsymbol{H}$ is necessary to obtain the original symbol sequences.

$$z_i(k + lN) = \sum_j H_{ij}(l) a_j(k + lN)$$
$$\Downarrow \text{ in matrix notation}$$
$$\bar{z}(k + lN) = \boldsymbol{H}(l)\, \bar{a}(k + lN) \tag{4.3}$$
$$\Downarrow$$
$$\bar{a}(k + lN) = \boldsymbol{H}(l)^{-1}\, \bar{z}(k + lN)$$

Again, this requires the receiver to estimate the channel. Note however that the number of coefficients that need to be estimated increases quadratically with the number of antennas: for an $N \times N$ MIMO system, N^2 coefficients need to be known. Additionally, the channel matrix can not be singular in order for this scheme to work. This can occur whenever the reception on both antennas is too strongly correlated. In this case, the receiver will not be able to separate the two spatial streams from both antennas and reception will fail. Here, a spatial stream is a term used in IEEE802.11 to describe the separate data streams in a MIMO channel, which corresponds to the signals sent on each transmit antenna in the example from earlier.

For a more theoretical description of a MIMO channel, the singular value decomposition of the channel matrix can be used. The channel matrix is always a square matrix, where the dimensions are determined by $\min(N_{a,r}, N_{a,t})$, with $N_{a,r}$ and $N_{a,t}$ the number of antennas at the receiver and the transmitter, respectively. The singular value decomposition of the channel matrix is given on equation (4.4). Here, the matrices $\boldsymbol{U}$, $\boldsymbol{\Sigma}$ and $\boldsymbol{V}$ are square matrices with the same dimensions as $\boldsymbol{H}$. $\boldsymbol{V}^H$ is the hermitian transpose of $\boldsymbol{V}$. Both $\boldsymbol{U}$ and $\boldsymbol{V}$ are complex unitary matrices, whereas $\boldsymbol{\Sigma}$ is a complex diagonal matrix. Remember that a unitary matrix $\boldsymbol{X}$ is characterized by the property $\boldsymbol{X}\boldsymbol{X}^H = \boldsymbol{X}^H\boldsymbol{X} = \boldsymbol{I}$. Also note that in equation (4.4) the index l indicating the subcarrier index is left out for the sake of brevity.

$$\boldsymbol{H} = \boldsymbol{U} \cdot \boldsymbol{\Sigma} \cdot \boldsymbol{V}^H \tag{4.4}$$

The diagonal values of $\boldsymbol{\Sigma}$ are called the singular values of the channel matrix $\boldsymbol{H}$. Since $\boldsymbol{U}$ and $\boldsymbol{V}$ are unitary matrices, the performance of a MIMO channel is entirely determined by these

singular values. Using the notation $\sigma_i = (\boldsymbol{\Sigma})_{i,i}$, figure 4.2 shows that due to the singular value decomposition, the MIMO channel can be treated equivalently as multiple SISO channels in parallel.
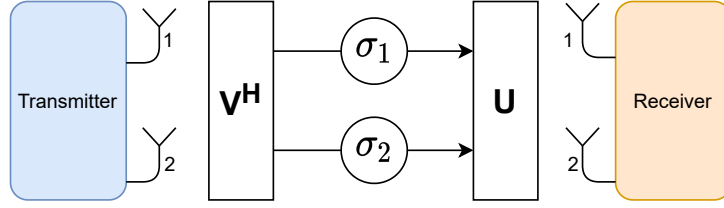

Figure 4.2: Singular value decomposition for a 2×2 MIMO channel

Each of the parallel SISO channels will thus contribute to the total capacity with a value given by Shannon's Law. However, in order for MIMO transmission to work, the singular values σ_i cannot be zero, as in this case the number of parallel SISO channels will be reduced. The relevant metric in this case is the rank of the channel matrix, which is equal to the number of non-zero singular values. In order for an $N \times N$ MIMO transmission to work, the rank of the corresponding channel matrix thus needs to be at least N.

Additionally, for MIMO to reach the full available capacity of the channel, another requirement is imposed on the singular values σ_i. This can be deducted from the equivalent channel formed by the singular value decomposition, which is shown in equation (4.5). In this derivation, a noise term $\bar{n}$ was added to the result from equation (4.3), and the symbol indexes were left out as well. Here, $\bar{n}$ is a vector of circularly symmetric and uncorrelated normal variables, with $E[\bar{n}\bar{n}^H] = \sigma_n^2 \boldsymbol{I}$.

$$
\begin{aligned}
\bar{z} &= \boldsymbol{H} \cdot \bar{a} + \bar{n} \\
&\Downarrow \\
\bar{z} &= \boldsymbol{U} \cdot \boldsymbol{\Sigma} \cdot \boldsymbol{V}^H \cdot \bar{a} + \bar{n} \\
&\Downarrow \boldsymbol{U}^H \boldsymbol{U} = \boldsymbol{I} \\
\boldsymbol{U}^H \cdot \bar{z} &= \boldsymbol{\Sigma} \cdot \boldsymbol{V}^H \cdot \bar{a} + \boldsymbol{U}^H \bar{n} \\
&\Downarrow \\
\bar{z}_{eq} &= \boldsymbol{\Sigma} \cdot \bar{a}_{eq} + \bar{n}_{eq}
\end{aligned}
\tag{4.5}
$$

Even though the information contained in $\bar{z}_{eq}$ and $\bar{z}$, and $\bar{a}_{eq}$ and $\bar{a}$ is not the same, the capacity of the equivalent channel will still be the same as the original channel. This is due to the fact that the statistics of the equivalent noise $\bar{n}_{eq}$ are equal to those of the original $\bar{n}$, and also due to the fact that matrices $\boldsymbol{U}$ and $\boldsymbol{V}$ are unitary matrices. The advantage of the equivalent channel is however that it can be treated as multiple parallel SISO channels, which makes calculating the channel capacity easier, as this can be obtained as the sum of the individual SISO channel capacities.

$$
\text{SNR}_i = \frac{\sigma_i^2 E_s}{\sigma_n^2} \qquad \rightarrow \qquad C = \sum_i \log_2 \left(1 + \text{SNR}_i\right) \tag{4.6}
$$

The capacity of all SISO channels together is given by equation (4.6). It can be seen that the maximal channel capacity will be obtained when all singular values are equal. One of the metrics for the channels quality is thus given by the condition of the channel matrix: this is equal to the ratio of the largest to the smallest singular value. A well-conditioned matrix corresponds to a value of 1. With increasing condition of the channel matrix, the SNR on some of the paths will be reduced, and decoding the weaker path becomes more difficult.

2 MIMO in IEEE802.11n

In IEEE802.11n, MIMO is used in some of the modulation and coding scheme (MCS) that are defined for transmission. An MCS defines the coding rate and type of modulation (e.g. BPSK or 4QAM), as well as the number of spatial streams. In IEEE802.11 terminology, a spatial stream corresponds to the number of MIMO streams that are used: this number will thus determine the dimensions of the channel matrix.

In order for the receiver to estimate this channel matrix, again one of the preambles can be used. The format of the full physical layer frame (PPDU) is shown in figure 4.3 for HT mixed mode, which is the format relevant to implementation on the openwifi platform. The HT part of the frame is preceded by legacy preamble and signal field, which can be used by receivers that do not support 802.11n to still obtain information about how long the channel will be used for. The information in the L-SIG and HT-SIG parts of the preamble is not yet sent using MIMO, since the receiver needs to know the correct number of spatial streams before channel estimation can be performed, which is included in the HT-SIG field. The part relevant to the MIMO channel estimation are the HT-LTF fields. Here, the number of data HT-LTFs needs to be equal to the number of spatial streams being used. The extension HT-LTFs can be used to estimate additional spatial streams of the channel which are not used for the current transmission.
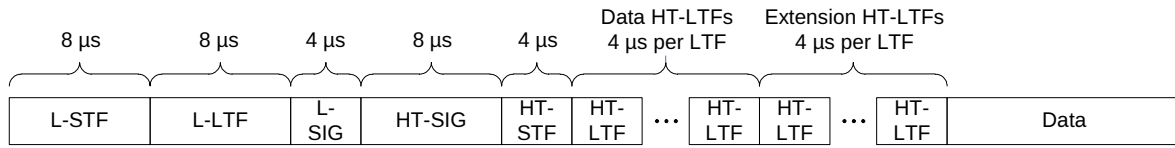
Figure 4.3: HT mixed format [10, p. 2347]

In what follows, an example will be given on how the channel matrix $\boldsymbol{H}$ can be derived from the HT-LTF in case of a 2×2 channel configuration. Since two spatial streams are used, the number of data HT-LTFs during the preamble is equal to two. In equation (4.7), the signal received on each antenna is shown during both HT-LTFs. In this expression, i represents the subcarrier index in a total of N subcarriers. L is equal to the HT-LTF sequence in the frequency domain, which is given in [10, p. 2370]. The signal received on antenna j after applying the operations from figure 2.5 is given by z_j, which is a sequence of $2N$ numbers.

$$\underbrace{\begin{bmatrix} z_1(i) & z_1(N+i) \\ z_2(i) & z_2(N+i) \end{bmatrix}}_{2\times 2} = \underbrace{\begin{bmatrix} H_{11}(i) & H_{21}(i) \\ H_{12}(i) & H_{22}(i) \end{bmatrix}}_{2\times 2} \cdot \underbrace{\begin{bmatrix} L(i) & -L(i) \\ L(i) & L(i) \end{bmatrix}}_{2\times 2} \quad \text{with } i = 0, 1, \ldots, N-1 \quad (4.7)$$

Note that in order to estimate the channel matrix, the second HT-LTF sequence on spatial stream 1 has been inverted. The receiver can then apply the inverse of the matrix representing the HT-LTF sequences on each spatial stream and extract the channel matrix. This is represented by equation (4.8). The factor $1/2$ is obtained by calculating the inverse of the HT-LTF matrix: since $L(i)$ is always either 1 or -1, the determinant of the HT-LTF matrix is always 2.

$$\frac{1}{2} \begin{bmatrix} z_1(i) & z_1(N+i) \\ z_2(i) & z_2(N+i) \end{bmatrix} \cdot \begin{bmatrix} L(i) & L(i) \\ -L(i) & L(i) \end{bmatrix} = \begin{bmatrix} H_{11}(i) & H_{21}(i) \\ H_{12}(i) & H_{22}(i) \end{bmatrix} \quad \text{with } i = 0, 1, \ldots, N-1 \quad (4.8)$$

3 Implementation

For implementation on the openwifi SDR board, the choice was made to implement the MIMO transmitter only. Since the used openwifi board only has 2 transmit antennas, this comes down to the implementation of MCS 8 to 15. There are also other MCS with 2 spatial streams, but those use different types of modulation on both spatial streams. A list of properties of each of these MCS is given in appendix A.

In order to support transmission at MCS 8 to 15, the *openofdm_tx* module from figure 3.1 needs to be modified. The complete block diagram of this module is shown on figure 4.4. Compared to the CSD implementation from chapter 3, now each antenna needs its own constellation mapper and IDFT block to support the two spatial streams. On the second spatial stream, the standard specifies that CSD can be used. The implementation of CSD from the previous chapter can be reused for this purpose. The use of CSD here can not really be called diversity, as now different signals are sent from both antenna. The benefit of CSD is now that it can help avoiding that the channel matrix becomes singular as the paths from both spatial streams become too similar.
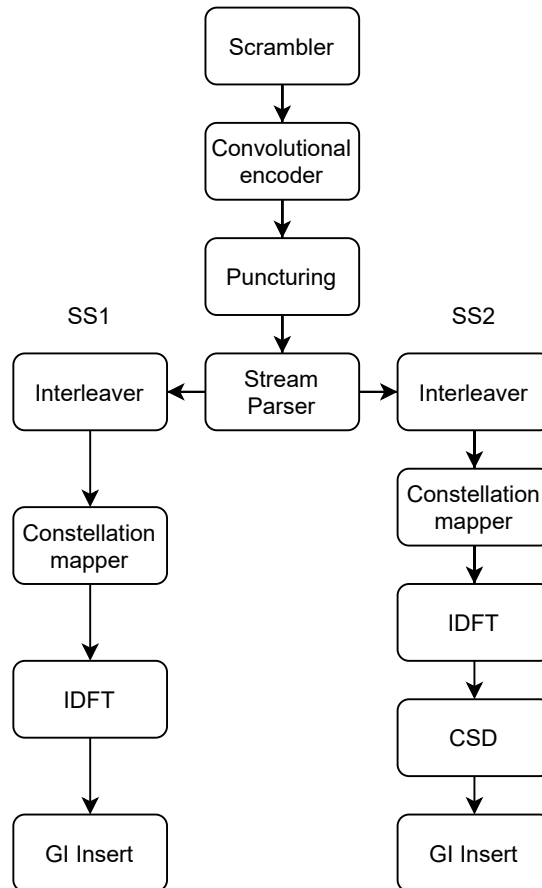
Figure 4.4: IEEE 802.11n transmitter block diagram for 2×2 MIMO operation

Remark that figure 4.4 is modified from the transmitter block diagram in the IEEE 802.11 standard [10, p.2350] in order to better represent the implementation on the openwifi platform. More specifically, only a single convolutional encoder is necessary in case only two spatial streams are used. Also, no STBC is applied. Lastly, the standard also suggests that spatial mapping can be used. Spatial mapping corresponds to the assignment of the spatial streams

to each of the antennas. The following options are specified in the IEEE 802.11 standard [10, p. 2387]:

Direct mapping The spatial streams are directly mapped onto a single transmit antenna

Indirect mapping The spatial streams are mapped onto the different transmit antennas by means of a matrix multiplication. A suggested example is the Fourier matrix. For a 2×2 system this matrix is equal to:

$$\begin{bmatrix} 1 & -1 \\ 1 & 1 \end{bmatrix}$$

Note that the mapping happens in the frequency domain, before the execution of the IDFT.

Spatial expansion This type of mapping is only used in case the number of spatial streams exceeds the number of available transmit antennas.

Beamforming IEEE 802.11 also specifies a system for closed-loop feedback between communicating nodes. Before transmission, the transmitter can then determine the spatial mapping matrix to be used based on the channel coefficients as estimated by the receiver. This way, the MIMO channel between both nodes can be improved.

In the MIMO implementation on the openwifi platform, direct mapping will be used. The reason for not using any other type of spatial mapping is that then the CSD implementation from chapter 3 would not be reusable. Indeed, spatial mapping requires that the CSD operation is performed in the frequency domain, instead of in the time domain corresponding to the cyclic shift operation from chapter 3.

From figure 4.4, the scrambler and convolutional encoder operations can be reused from the original *openofdm_tx* module. The convolutional encoder is shown on figure 4.5. This encoder works at a coding rate of $1/2$, but other coding rates can be achieved by puncturing. In the openwifi design, the output of the convolutional encoder is first written into a FIFO queue, which makes the subsequent puncturing operation easier.
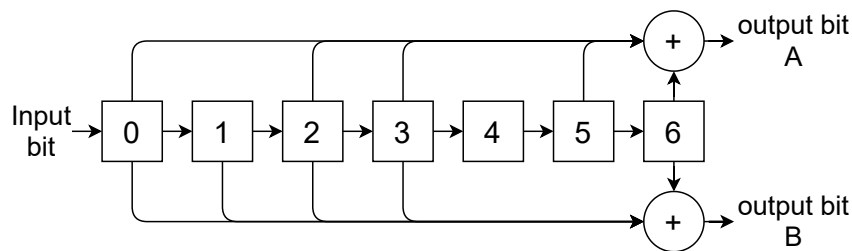
Figure 4.5: Convolutional encoder used in IEEE 802.11 [10, p. 2295]

In the unmodified *openofdm_tx* module, puncturing and interleaving are performed simultaneously by using a lookup table (LUT). For puncturing, this LUT provides the necessary info on which bits need to be left out (punctured) at the output of the encoded bits FIFO. The interleaving operation is performed by writing the punctured bits to a memory for which the address is provided by this LUT. The input of the subsequent constellation mapping can then be obtained by reading from this memory in linear fashion.

In the table of MCS listed in appendix A, it can be seen that there are four different coding rates. The puncturing pattern for each of these coding rates is given on figure 4.6. Note that

A_0	A_1	A_2	A_3	A_4	A_5
B_0	B_1	B_2	B_3	B_4	B_5

(a) $\frac{2}{3}$

A_0	A_1	A_2	A_3	A_4	A_5	A_6	A_7	A_8
B_0	B_1	B_2	B_3	B_4	B_5	B_6	B_7	B_8

(b) $\frac{3}{4}$

A_0	A_1	A_2	A_3	A_4
B_0	B_1	B_2	B_3	B_4

(c) $\frac{5}{6}$

Figure 4.6: Puncturing for the different coding rates [10, p.2296, p.2377]

coding rate 1/2 is not listed as no puncturing is required in this case. The corresponding timing diagram for puncturing is shown on figure 4.7. Here, the *bits_enc* signal corresponds to the output of the FIFO queue, which outputs 2 coded bits at a time. The *punc_info* signal is given by the output of a LUT, of which the out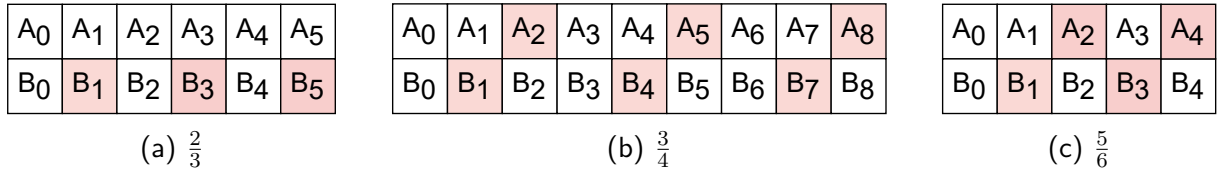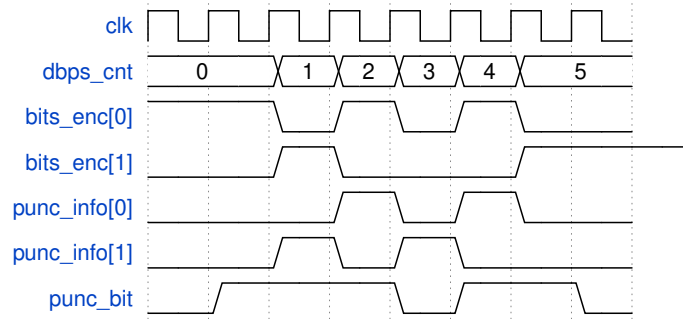put is determined by the *dbs_cnt* signal. Finally, the puncturing bit is then chosen as one of the two *bits_enc* bits, based on the *punc_info* signal. Note that the FIFO queue is not read for a single clock cycle in case no puncturing occurs for the current code bit. In this case, bit A from figure 4.5 is output before bit B.

Figure 4.7: Puncturing timing diagram for coding rate $\frac{5}{6}$

After puncturing, stream parsing can be performed. The stream parser will assign a number of consecutive, punctured bits to each spatial stream in a round robin fashion [10, p. 2382]. The number of consecutively assigned bits is determined by the used constellation, and is given by equation (4.9). Here, $N_{BPSCS}(i_{SS})$ is equal to the number of coded bits per subcarrier on spatial stream i_{SS}. As an example, when using MCS 12 for transmission, which uses 16-QAM, 2 bits will be alternately assigned to each spatial stream.

$$s(i_{SS}) = \max\left(1, \frac{N_{BPSCS}(i_{SS})}{2}\right) \tag{4.9}$$

Next, interleaving the bits assigned to each spatial stream will reorder the bits in order to obtain a better burst error correction capability. The interleaving operation is defined using three different permutations [10, p. 2383], which are repeated in equations (4.10) to (4.12). On each spatial stream, bits with index i will thus be reordered to index r. Indices i, j and r go from 0 to $N_{CBPSS}(i_{SS}) - 1$. For an overview of the definition of the used symbols, see appendix A.

$$i = N_{ROW} \times (k \bmod N_{COL}) + \lfloor k/N_{COL} \rfloor \tag{4.10}$$

$$j = s \times \lfloor i/s \rfloor + (i + N_{CBPSS}(i_{SS}) - \lfloor N_{COL} \times i/N_{CBPSS}(i_{SS}) \rfloor) \bmod s \tag{4.11}$$

$$r = \left(j - \left(((i_{SS} - 1) \times 2) \bmod 3 + 3 \times \left\lfloor \frac{i_{SS}}{3} \right\rfloor\right) \right. $$
$$\left. \times N_{ROT} \times N_{BPSCS}(i_{SS})\right) \bmod N_{CPBSS}(i_{SS}) \tag{4.12}$$

On the FPGA, stream parsing and interleaving are performed by a separate LUT from the puncturing LUT: this is different from the original design. The reason for splitting the three operations over two LUTs is that synthesis of a single LUT becomes more involved as the LUT grows with the extended number of values that need to be output to support more MCS. In the modified openwifi design, the puncturing operation is performed by an asynchronous LUT, whereas the stream parsing and interleaving signals are provided by a separate, synchronous LUT. By making the LUT synchronous, some of the combinatorial paths will be shortened, which makes synthesis easier.

As a side note, the interleaved bit indices obtained from equations (4.10) to (4.12) are also adapted such that the bits corresponding to a constellation symbol are byte-aligned. This also makes synthesis easier, as the memory that the interleaved bits are written to can then be read one byte at a time.

On figure 4.8, an example timing diagram is shown for the stream parsing and interleaving operation at MCS 15. Since the corresponding constellation is 64-QAM, $s(i_{SS})$ is equal to 3 for all spatial streams, and 3 bits are alternately assigned to spatial stream 1 or 2. The *streamp_info* and *interlv_addr* signals are the output of the previously mentioned LUT. The *dbps_cnt* signal counts each of the data bits, and is used as an input to the LUT. Note that the LUT is synchronous, so a change in *dbps_cnt* only results in a change in the output during the next clock cycle.
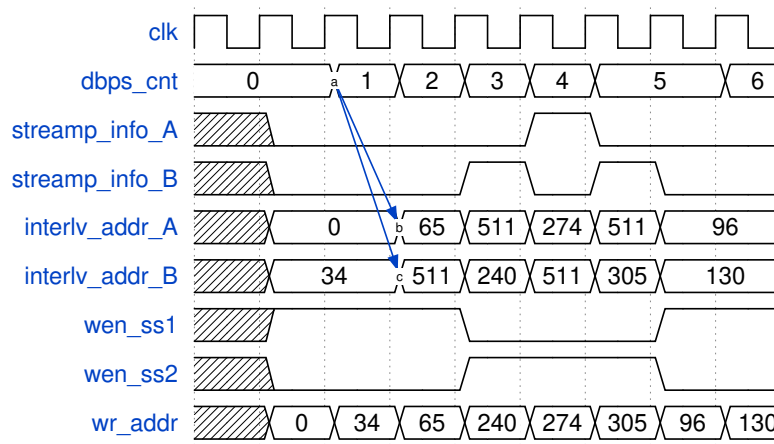

Figure 4.8: Timing diagram for stream parsing and interleaving (example at MCS 15)

Next to the modifications in the openwifi design in the data path, some additional logic needs to be introduced as well. One such addition is the need to send a second HT-LTF during the preamble. Note that this second HT-LTF needs to be inverted for the first spatial stream, as was shown in the example from equation (4.7). The structure from figure 3.11 is still applicable for the MIMO implementation, but now the ROMs mentioned on that figure have been made synchronous. This is mainly needed during the second HT-LTF, as the inversion that needs to be applied to the output of the corresponding ROM for spatial stream 1 is not possible in a single clock cycle.

Another modification concerns the pilot symbols that are included on specific subcarriers (see figure 2.9) inside each OFDM symbol. In case two spatial streams are used, the polarity of these symbols is different than when only a single spatial stream is used. The correct start sequence for each situation is listed in table A.5. This is the polarity which is used for the first data OFDM symbol. In subsequent symbols, the correct polarity is obtained by cyclically

shifting between the pilot subcarriers [10, p.2385]. Note that in case two spatial streams are used, the pilot polarities of the second spatial stream are also a cyclically shifted version of the first spatial stream. On the FPGA, this implies that only the polarities of a single spatial stream has to be tracked, as the polarities for the other spatial stream can always be obtained by a cyclical shift. The final pilot polarity to be inserted between data symbols before the IDFT is obtained by multiplying the correctly shifted values from table A.5 with a sequence generated by a scrambler [10, p.2390]. This is similar to how the pilot polarity is calculated for legacy operation.

Next to the modifications on the FPGA, an additional change is needed in the SDR driver (see figure 3.1) to let the Linux *mac80211* subsystem know that now also MCS 8-15 can be used for transmission. This change is quite small, as the functionality used to choose the transmit rate is entirely handled by the *mac80211* layer, and more specifically the *minstrel* rate selection algorithm. The supported set of MCS can be indicated as defined in the standard [10, p.944]. Unfortunately, the *mac80211* layer assumes that the rates used for transmission should also be supported for reception, which has not yet been implemented on the openwifi board. In order to trick the *mac80211* subsystem into using MCS 8-15, support for both reception and transmission of MIMO with 2 spatial streams has to be indicated. For further measurements, this implies that the uplink to the openwifi board might become less reliable, as the other side might try to transmit with a MCS which can not be received by the openwifi board.

4 Measurements

In order to verify the working of the new MCS, the throughput is measured from the openwifi board to a laptop running Linux with an 'Intel Dual Band Wireless 8265' chip using the *iperf* utility. A picture of the measurement setup is shown in figure 4.9. Note that the monitor is relatively close to the setup. As such, additional multipath will be introduced, which should make it less likely that the channel matrix seen by the laptop becomes ill-conditioned. The throughput is measured over UDP, since the obtained result over TCP would not be reliable due to the additional acknowledgements that need to be sent from the laptop to the openwifi board. When the openwifi board is restricted to the use of MCS 0-7, a throughput of 33,1 Mbits/sec is obtained. Note that in this case still two antennas where used, with CSD activated on the second antenna as show in chapter 3. After allowing the openwifi board to also use MCS 8-15, the measured throughput increased to 44,8 Mbits/sec. The corresponding *iperf* screenshot is shown in figure 4.10.
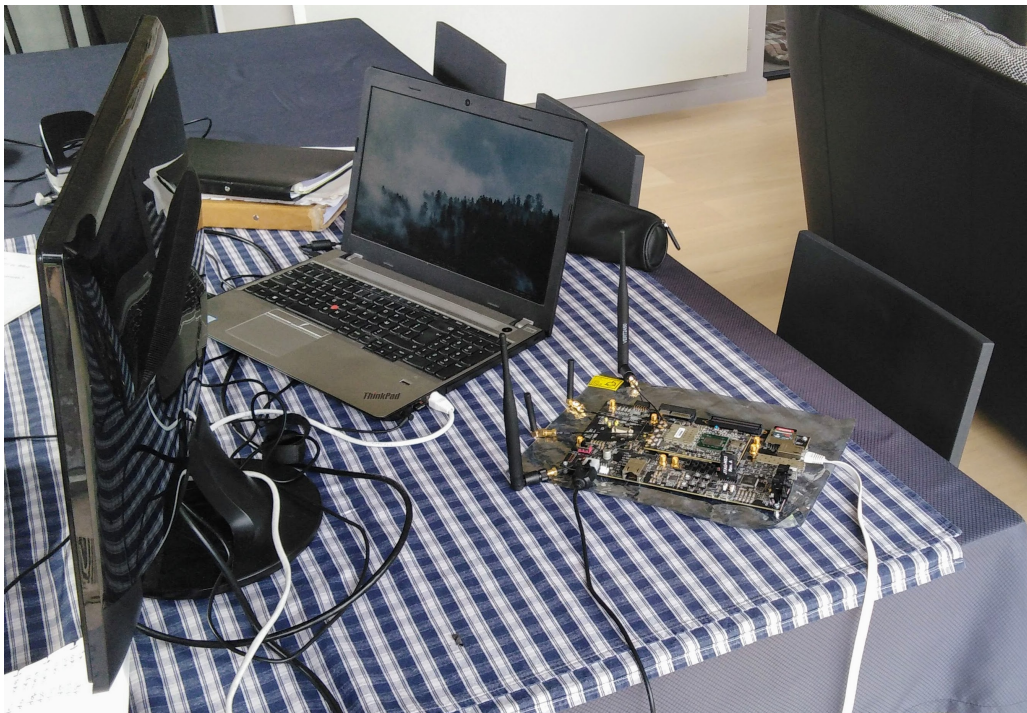

Figure 4.9: Home measurement setup

Figure 4.10: Screenshot of change in *iperf* throughput after disabling MIMO

Although this is not a doubling of the throughput, the obtained result is what is to be expected for end-to-end UDP traffic over 802.11n. To illustrate this, the expected throughput can be calculated. For the situation where the UDP throughput is measured using *iperf*, the timing to send a single IEEE 802.11 packet over the channel is given on figure 4.11. The transmission duration for a single packet is given by T_p. After reception of a packet, the receiver waits for the duration of a SIFS before sending an acknowledgement back to the receiver. The SIFS duration for 802.11n in the 5 GHz band is equal to 16 µs [10, p.2426].

For the transmission of an acknowledgement, the frame structure from figure 4.3 is used, where the acknowledgement data takes around 14 bytes [10, p.638]. By verifying through *tcpdump* on the openwifi board, it was found that the majority of the acknowledgements coming from the laptop were sent at the legacy rate of 18 Mbits/s. The preamble for such a legacy packet is only 20 µs long, as only the L-STF, L-HTF and L-SIG from figure 4.3 need to be included. At a rate of 18 Mbits/s, the 14 bytes of the acknowledgement correspond to 2 OFDM symbols of 4 µs. The total acknowledgement time is then equal to 28 µs.

Before another packet can be sent by the transmitter, it has to wait for a predefined time given by the DIFS, and a random contention period in other to allow other nodes to contend for the medium in case they would like to transmit as well [10, p.1306]. The DIFS time is given by the SIFS time and two times the slot time [10, p.1332]. For operation within the 5 GHz band, this corresponds to a time of 34 µs. Finally, the contention window (CW) time needs to be approximated, as this value is chosen at random as a number of slot times. In the case where only the laptop is connected to the openwifi board, the contention window will generally be small, as no other nodes need to access the medium. The CW can be approximated by assuming that on average, a window size between 0 and the minimal contention window will be chosen. The minimal contention window for 802.11n in the 5 GHz band is equal to 15 times the slot size (9 µs) [10, p.2426]. On average, the contention window will thus be around 7·9=63 µs.

Packet	SIFS	ACK	DIFS	CW
T$_p$	16 µs	28µs	34 µs	63 µs

Figure 4.11: Time durations for throughput calculation

The packet duration T_p will differ according to which MCS is used for transmission. For MCS 7, the preamble will take 36 µs (see figure 4.3). For MCS 15, the preamble will be 4 µs longer due to the need for the additional HT-LTF to support 2 spatial streams. The data transmitted by *iperf* has a size of 1470 bytes. The total packet size, with UDP header of 8 bytes, IPv4 header of 20 bytes and LLC header of a single byte, is then equal to 1499 bytes. The corresponding calculation for T_p is given below. The data rates correspond to those in appendix A, where a short GI is used. Note that T_p has to be rounded to a multiple of 3,6 µs, which is the duration of an OFDM symbol in case a short GI is used.

MCS 7   MCS 15

$$T_p = 36 + \left\lceil \frac{1499 \cdot 8\,\text{bits}}{72{,}2\,\text{Mbits/s}} \right\rceil_{3,6\,\mu s} = 205{,}2\,\mu s \qquad T_p = 40 + \left\lceil \frac{1499 \cdot 8\,\text{bits}}{144{,}4\,\text{Mbits/s}} \right\rceil_{3,6\,\mu s} = 126{,}4\,\mu s$$

The total throughput as measured by *iperf* can then be estimated as below:

$$\frac{1499 \cdot 8 \text{ bits}}{(205{,}2 + 16 + 28 + 34 + 63)\,\mu\text{s}}$$

$$\approx 34{,}6 \text{ Mbits/s}$$

$$\frac{1499 \cdot 8 \text{ bits}}{(126{,}4 + 16 + 28 + 34 + 63)\,\mu\text{s}}$$

$$\approx 44{,}8 \text{ Mbits/s}$$

The throughput as measured on the openwifi board thus corresponds to the expected improvement by introducing MIMO transmission.

Chapter 5

Conclusion and outlook

In this thesis, several methods of using multiple antennas in the 802.11 standard have been discussed and implemented on the openwifi platform. These implementations were then also verified in end to end communication. Firstly, the use of spatial diversity was demonstrated for both reception and transmission. At the receiver, the equal gain combining scheme was applied on the openwifi platform, and evaluated in a controlled environment. It was shown that the reliability of the wireless communication is improved by combining the signals coming from the different antennas. At the transmitter, the use of cyclic shift diversity (CSD) is discussed and evaluated in the same controlled environment. Measurements showed that by using cyclic shift diversity, additional frequency selectivity is introduced, and unintentional beamforming can be avoided. Next, the use of spatial multiplexing (MIMO) was added to the openwifi transmitter, and evaluated in a real life setup. It is shown that the measured increase in throughput corresponds to the expected improvement in an 802.11n setting.

Since MIMO will most likely become more and more prevalently used in 802.11 standards, future work on the openwifi platform could include the support for reception of MIMO, as well as support for MU-MIMO which is included in the new Wi-Fi 6 standard. But new technologies that help to increase the maximum achievable throughput at the physical layer are not always as useful, as other factors can have more influence on the actual throughput experienced by end users. Firstly, this is due to the fact that the channel between communicating nodes needs to support the higher rates, which is not always the case. Approaches such as the spatial diversity from chapter 3 might make more sense in that case. Another reason why the actual throughput often largely differs from the maximum physical layer bitrate, is the contention based medium access control mechanism. With the development of Wi-Fi 6, the contention based approach was scrapped in favour of orthogonal frequency division multiple access (OFDMA) for medium access control, which removes much of the congestion when multiple nodes need to communicate at the same time. Implementation of the new OFDMA based access scheme requires lots of modifications on the openwifi platform, but could also be a possible extension of the currently supported set of features.

Since the SDR boards used by the openwifi platform are limited to two antennas, further extension to massive MIMO does not seem feasible. However, instead of employing a large number of antennas on a single board, it is also possible to move to a distributed massive MIMO approach, where a large number of antennas are spread out over different locations. This approach is known as cell free massive MIMO. The cell free massive MIMO concept is

currently not yet used in any standard, but is cited as one of the technologies behind the development of 6G cellular networks. The design of cell free networks brings new challenges that still need to be addressed, such as the need for accurate time synchronization, and the requirement for a low-latency, high-rate connection between the participating nodes to perform the distributed signal processing [22]. Since openwifi is not limited to technologies that are already defined in existing standards, the platform could be used to test and evaluate the performance of the cell free massive MIMO approach.

To conclude, the openwifi platform offers many possibilities for research on the improvement of 802.11 networks. In this thesis, the advantages of spatial diversity and multiplexing have been demonstrated. As such, the use of multiple antennas has been introduced to the openwifi platform. Future research on multi-antenna systems can benefit from the open source nature of the openwifi platform to further experiment with state-of-the-art features for application in new standards.

Bibliography

[1] W. Liu, X. Jiao, P. Becue, S. Pollin, T. Vermeulen, S. A. Hassani, A. Guevara, and C. Felber, "D2.2: Technical requirements of the ORCA test facility," 2017.

[2] I. Gomez-Miguelez, A. Garcia-Saavedra, P. D. Sutton, P. Serrano, C. Cano, and D. J. Leith, "srsLTE: An open-source platform for LTE evolution and experimentation," vol. 03-07-October-2016, Association for Computing Machinery, Oct. 2016, pp. 25–32, ISBN: 9781450342520. DOI: 10.1145/2980159.2980163. [Online]. Available: https://dl.acm.org/doi/10.1145/2980159.2980163.

[3] *Openairinterface*. [Online]. Available: https://openairinterface.org/ (visited on Feb. 22, 2021).

[4] X. Jiao, W. Liu, and M. Mehari. "Open-source IEEE802.11/Wi-Fi baseband chip/FPGA design." (2019), [Online]. Available: https://github.com/open-sdr/openwifi.

[5] M. Cominelli, F. Kosterhon, F. Gringoli, R. L. Cigno, and A. Asadi, "An experimental study of CSI management to preserve location privacy," in *Proceedings of the 14th International Workshop on Wireless Network Testbeds, Experimental Evaluation & Characterization*, ser. WiNTECH'20, London, United Kingdom: Association for Computing Machinery, 2020, pp. 64–71, ISBN: 9781450380829. DOI: 10.1145/3411276.3412187. [Online]. Available: https://doi.org/10.1145/3411276.3412187.

[6] *The mac80211 subsystem kernel documentation*. [Online]. Available: https://www.kernel.org/doc/html/v4.9/80211/mac80211.html (visited on Mar. 4, 2021).

[7] S. B. Weinstein, "The history of orthogonal frequency-division multiplexing [history of communications]," *IEEE Communications Magazine*, vol. 47, no. 11, pp. 26–35, 2009. DOI: 10.1109/MCOM.2009.5307460.

[8] G. Ou. "Is airgo the uncrowned king of 802.11n mimo? — zdnet." (Jun. 2005), [Online]. Available: https://www.zdnet.com/article/is-airgo-the-uncrowned-king-of-802-11n-mimo (visited on Feb. 13, 2021).

[9] R. Chataut and R. Akl, "Massive mimo systems for 5G and beyond networks—overview, recent trends, challenges, and future research direction," *Sensors*, vol. 20, no. 10, 2020, ISSN: 1424-8220. DOI: 10.3390/s20102753. [Online]. Available: https://www.mdpi.com/1424-8220/20/10/2753.

[10] "IEEE Standard for Information technology—Telecommunications and information exchange between systems Local and metropolitan area networks—Specific requirements - Part 11: Wireless LAN Medium Access Control (MAC) and Physical Layer (PHY) Specifications," *IEEE Std 802.11-2016 (Revision of IEEE Std 802.11-2012)*, 2016. DOI: 10.1109/IEEESTD.2016.7786995.

[11] H. Rogier, "Antennas and Propagation," Course syllabus, 2019.

[12] M. Moeneclaey and L. Jacobs, "Modulation and Detection," Course syllabus, 2020.

[13] B. Gupta, G. Gupta, and D. S. Saini, "BER performance improvement in OFDM system with ZFE and MMSE equalizers," in *2011 3rd International Conference on Electronics Computer Technology*, vol. 6, 2011, pp. 193–197. DOI: 10.1109/ICECTECH.2011.5942079.

[14] D. Mitić, A. Lebl, T. Branimir, and Z. Markov, "An overview and analysis of BER for three diversity techniques in wireless communication systems," *Yugoslav Journal of Operations Research*, vol. 25, pp. 7–7, Jan. 2014. DOI: 10.2298/YJOR131120007M.

[15] D. Xia, J. Hart, and Q. Fu, "On the performance of rate control algorithm minstrel," 2012, pp. 406–412, ISBN: 9781467325691. DOI: 10.1109/PIMRC.2012.6362819.

[16] A. Wittneben, "A new bandwidth efficient transmit antenna modulation diversity scheme for linear digital modulation," in *Proceedings of ICC '93 - IEEE International Conference on Communications*, vol. 3, 1993, 1630–1634 vol.3. DOI: 10.1109/ICC.1993.397560.

[17] S. Kaiser, "Spatial transmit diversity techniques for broadband OFDM systems," in *Globecom '00 - IEEE. Global Telecommunications Conference. Conference Record (Cat. No.00CH37137)*, vol. 3, 2000, 1824–1828 vol.3. DOI: 10.1109/GLOCOM.2000.891949.

[18] A. Dammann and S. Kaiser, "Performance of low complex antenna diversity techniques for mobile ofdm systems," Jan. 2001, ISBN: 978-1-4419-4945-5. DOI: 10.1007/978-1-4757-3569-7_6.

[19] *Kernel documentation on ath9k spectral scan*. [Online]. Available: `https://wireless.wiki.kernel.org/en/users/drivers/ath9k/spectral_scan` (visited on May 3, 2021).

[20] "5 GHz RLAN; harmonised standard covering the essential requirements of article 3.2 of directive 2014/53/EU," European Telecommunications Standards Institute, Valbonne, FR, Standard, May 2017.

[21] C. E. Shannon, "Communication in the presence of noise," *Proceedings of the IRE*, vol. 37, pp. 10–21, 1 1949, ISSN: 00968390. DOI: 10.1109/JRPROC.1949.232969.

[22] J. Zhang, S. Chen, Y. Lin, J. Zheng, B. Ai, and L. Hanzo, "Cell-free massive mimo: A new next-generation paradigm," *IEEE Access*, vol. 7, pp. 99 878–99 888, 2019. DOI: 10.1109/ACCESS.2019.2930208.

Appendix A

IEEE 802.11n values

Symbol	Explanation
R	Coding rate
N_{SS}	Number of spatial streams
$N_{BPSCS}(i_{SS})$	Number of coded bits per single carrier for each spatial stream, $i_{ss} = 1, \cdots, N_{SS}$
N_{CBPS}	Number of coded bits per OFDM symbol
N_{DBPS}	Number of data bits per OFDM symbol

Table A.1: Used symbols [10, p.2427]

MCS Index	Modulation	R	$N_{BPSCS}(i_{ss})$	N_{CBPS}	N_{DBPS}	Data rate (Mbits/s)	
						800ns GI	400ns GI
0	BPSK	1/2	1	52	26	6.5	7.2
1	QPSK	1/2	2	104	52	13.0	14.4
2	QPSK	3/4	2	104	78	19.5	21.7
3	16-QAM	1/2	4	208	104	26.0	28.9
4	16-QAM	3/4	4	208	156	39.0	43.3
5	64-QAM	2/3	6	312	208	52.0	57.8
6	64-QAM	3/4	6	312	234	58.5	65.0
7	64-QAM	5/6	6	312	260	65.0	72.2

Table A.2: MCS with single spatial stream [10, p.2427]

MCS Index	Modulation	R	$N_{BPSCS}(i_{ss})$	N_{CBPS}	N_{DBPS}	Data rate (Mbits/s)	
						800ns GI	400ns GI
8	BPSK	1/2	1	104	52	13.0	14.4
9	QPSK	1/2	2	208	104	26.0	28.9
10	QPSK	3/4	2	208	156	39.0	43.3
11	16-QAM	1/2	4	416	208	52.0	57.8
12	16-QAM	3/4	4	416	312	78.0	86.7
13	64-QAM	2/3	6	624	416	104.0	115.6
14	64-QAM	3/4	6	624	468	117.0	130.0
15	64-QAM	5/6	6	624	520	130.0	144.4

Table A.3: MCS with 2 spatial streams [10, p.2428]

Parameter	Value
N_{COL}	13
N_{ROW}	4 $N_{BPSCS}(I_{SS})$
N_{ROT}	11

Table A.4: Interleaver parameters for operation within 20 MHz channel [10, p.2383]

N_{SS}	i_{SS}	Pilot index			
		-21	-7	7	21
1	1	1	1	1	−1
2	1	1	1	−1	−1
2	2	1	−1	−1	1

Table A.5: Pilot polarity for 20 MHz transmission [10, p.2386]